DESIGN AND ANALYSIS OF A FREE POWER TURBINE

FOR AN AUXILIARY POWER UNIT

A Major Project Report Submitted as Partial Fulfillment of the

Requirement for the Award of Degree of

MASTER OF ENGINEERING

IN

THERMAL ENGINEERING

SUBMITTED BY:

RAM KUMAR SHARMA

UNDER THE GUIDANCE OF:

Dr. B.B.ARORA

Assistant Professor

DCE, Delhi

DEPARTMENT OF MECHANICAL AND PRODUCTION ENGINEERING

DELHI COLLEGE OF ENGINEERING

UNIVERSITY OF DELHI, DELHI-110042

SESSION 2006-09

CANDIDATE'S DECLARATION

I hereby declare that the work which being present in the major project entitled "**Design and Analysis of Free Power Turbine for an Auxiliary Power Unit**" in the partial fulfillment for the award of degree of MASTER of ENGINEERING with specialization in "THERMAL ENGINEERING" submitted to Delhi College of Engineering, University of Delhi, is an authentic record of my own work carried out under Academic supervision of **Dr. B.B.ARORA, Department of Mechanical Engineering, Delhi College of Engineering, University of Delhi**. I have not submitted the matter in this dissertation for the award of any other Degree or Diploma or any other purpose what so ever.

RAM KUMAR SHARMA

University Roll No: 12311

College Roll No. 08-THR-2006

CERTIFICATE

This is to certify that the above statement made by RAM KUMAR SHARMA is true to the best of our knowledge and belief.

Dr. B. B. ARORA

Assistant professor

Department of Mechanical Engineering

Delhi college of Engineering, Delhi

Acknowledgement

I would like to thank my advisor, Mr. A. Gogoi, Scientist, ADA, Bangalore for his guidance and support during the project and for permitting me to the use of ADA facilities and super computers and for his very constructive remarks on the writing of this thesis. Also, my special thanks go to my supervisors, Prof. B. B. Arora for his guidance and technical support for the project and the writing of the thesis. I feel privileged to have had such dedicated advisors with a flair for excellence.

Since the entire work of this thesis has been carried out at ADA, I would like to thank all the members of ADA, Propulsion Group and their leader Mr. H. Siddesha for his helpful technical expertise. Also I would like to express my gratitude to DCE team, and especially to Dr. Sagar Maji, for the helpful suggestions, and for his particular sense of humour.

Also, I would like to extend my thanks to our Director, Dr. P. B. Sharma to provide a nice and friendly environment at college that has inspired great work with camaraderie.

Last but not the least, I would like to express my extreme and deepest thanks to my wife Mrs. Sapna Sharma her continuous encouragement and support throughout my studies. Also, I would like to express my special thanks to all my friends.

Thus I would like to dedicate this modest work to my family and my motherland INDIA, the land of inspiration

Abstract

The next generation design of small gas turbines outshines the present capabilities in improved aerodynamics, superior technologies and high reliability to ensure air superiority and survivability. Auxiliary Power Units (APU's) are such small gas turbines that provide many benefits to the modern military aircrafts. The performance of the each individual component of an APU is therefore significant. Literature reports various efforts and state-of-art review made by many researchers in experimental and computational fields for the improvement of performance in each component involving compressor, combustor and especially that of a turbine. The design of a turbine stage that produces high performance is therefore essential to meet the requirements of APU.

The report presents design and analysis of a free power turbine stage for an auxiliary power unit. Preliminary free vortex based design, CFD analysis and mechanical analysis were carried out in an iterative manner and optimisation processes were incorporated at each step of detail design process. A preliminary design code was also developed in the course of the present work. The CFD software tool, FINE TURBO of NUMECA was validated to use for further studies by comparing the computational results with the experimental data of Aachen turbine. Appropriate grids of the turbine stage with desirable features like orthogonality, clustering, smoothness, etc were generated in Autogrid. CFD computations were carried out with the popular Spalart Allmaras turbulence model and the central difference Jameson scheme.

The results from the computational study were in excellent agreement with the preliminary design values and the turbine produced impressive efficiency even at lower specific speeds. Effect of various parameters, like tip clearance and blade stagger, which could not be addressed in the preliminary design, were studied through CFD analysis and optimum values of these parameters were obtained. The off-design performance evaluation was also performed through CFD and compared with loss modelling procedure reported in the literature. Design was also checked for mechanical integrity in terms of stress levels in the blisk using ANSYS. The blisk was found to be safe even with 15% overspeed, thus meeting the requirements as per Military standards.

Table of Contents

List of Figures

Nomenclature

Symbol	Unit	Description
A	mm^2	Cross-sectional area
C	-	Secondary loss coefficient
D	mm	Diameter
H	kJ/kg	Enthalpy
N	rpm	Rotational speed
T	K	Temperature
U	m/s	Blade speed
V	m/s	Absolute velocity
Y	-	Blade loss coefficient
c	mm	Chord
h	mm	Blade height
s	mm	Blade space
t	mm	Blade thickness
α	radians	Flow angle
β	radians	Blade angle

Abbreviations

APU	-	Auxiliary Power Unit
CFD	-	Computational Fluid Dynamics
FEA	-	Finite Element Analysis
GGT	-	Gas Generator Turbine
GTS	-	Gas Turbine Starter
HCF	-	High Cycle Fatigue
NGV	-	Nozzle Guide Vane
MIL	-	Military Standards

TIT - Turbine Inlet Temperature

1 – Introduction

1.1 An Introduction to Small Gas Turbines

Gas turbines are typical power sources used in a wide range of sizes for propulsion and power generation systems. Recently, there has been considerable interest shown in the research, development and application of small gas turbines to yield high power density at lower costs. However, resulting from the smaller size, their efficiency, pressure ratio and specific work are mostly lower than those of the large scale systems. Therefore, innovations are required to attractively enhance their performance.

At present, there are two major methods to enhance the performance of a simple cycle gas turbine viz., improving the component efficiencies, especially of compressor and turbine, or improving the thermodynamic process of the cycle by increasing the Turbine Inlet Temperature (TIT). From thermodynamics point of view, increasing the TIT is the most effective way to improve both the overall efficiency and the specific power. However, the maximum temperature of the gas entering the turbine is limited by the material considerations. Thus a considerable jump in the performance of small gas turbines can only be achieved by applying advanced thermodynamic processes that are not subjected to this limitation. Secondly, the advanced aerodynamics of turbomachinery has already resulted in very high level of component efficiencies of up to around 90%. Improvements still are possible, but further huge enhancements seem to be unlikely.

The design of a gas turbine engine is a fairly lengthy and complex process, involving many engineering disciplines like heat transfer, materials science, combustion, turbomachinery and structural science, apart from aerodynamics and thermodynamics. All these fields are employed while designing an appropriate engine configuration and thus it requires several months, and sometimes years, of detailed analyses and testing. A simplified schematic of a gas turbine design process is presented in Figure 1.1

Due to the massive competition in the gas turbine industry, and to the continuous

advances in design techniques, even a minor improvement in engine total efficiency can make lot of difference to the manufacturers in the trade. Because of this, the companies invest in R&D on each component of the gas turbine engine, subjecting it to extensive detailed analyses and experiments to achieve the maximum efficiency possible.

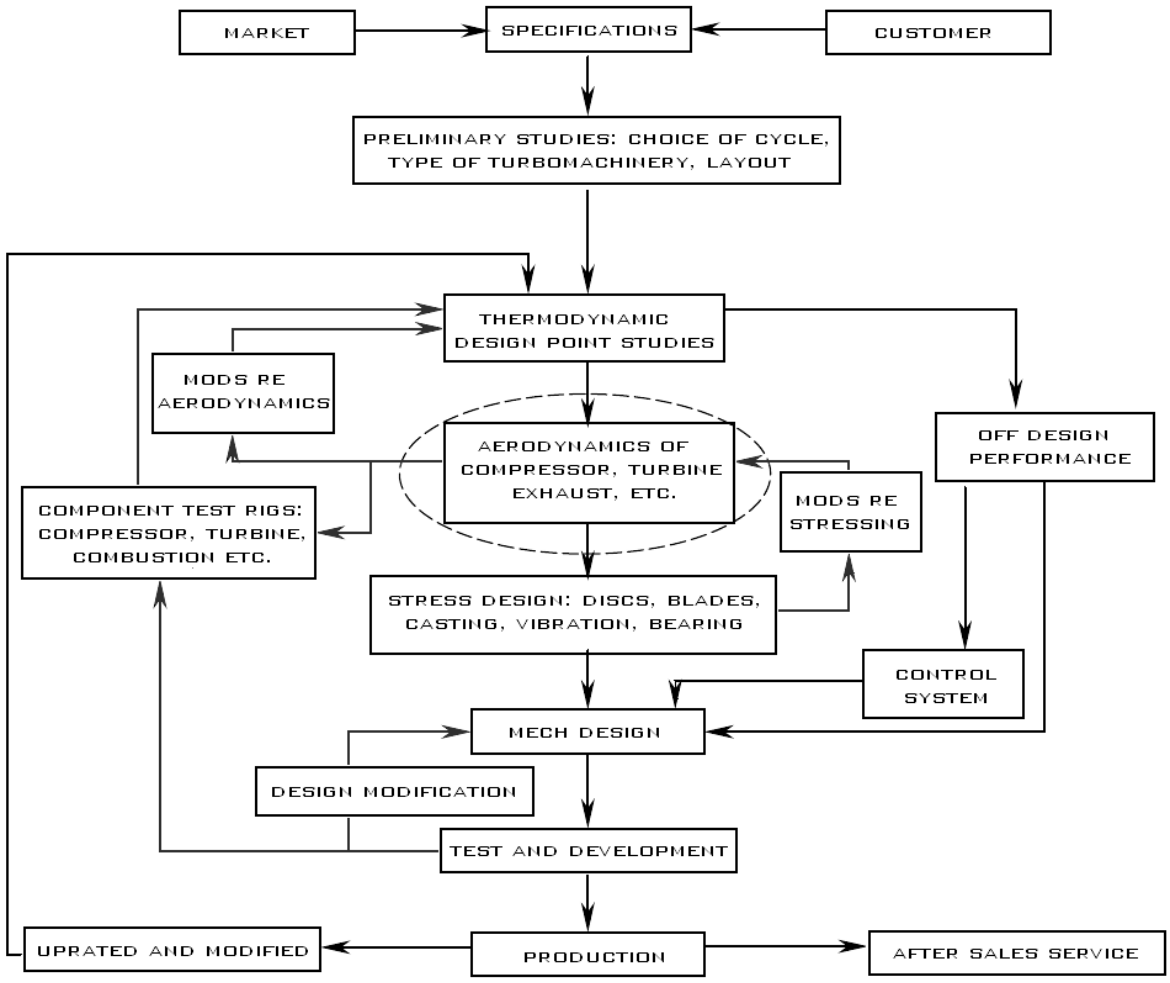

Figure 1.1 Gas Turbine Design Procedure [1]

One of the leading and expert organisations in the field of small gas turbine design and development is the Aeronautical Development Agency (ADA), India. It was a privilege to carry out the entire work of my present thesis in this Research & Development centre. As a sequel to the Light Combat Aircraft (LCA), a Multi-role Combat Aircraft (MCA) is proposed to be developed by ADA. It is felt that an Auxiliary Power Unit (APU) is absolutely necessary for the

MCA. The APU in the fighter aircrafts may be used for the following tasks:

- Starting the main engine on the ground
- In-flight re-start of the main engine
- Providing bleed air for cockpit and engine bay ventilation in air and on ground
- Providing power for various hydraulic and electrical systems in air & on ground

Figure 1.2 A Gas Turbine Starter [2]

Selection of architecture and modularity are other considerable tasks in an engine design process. Preliminary studies and experiments have revealed that selecting a centrifugal

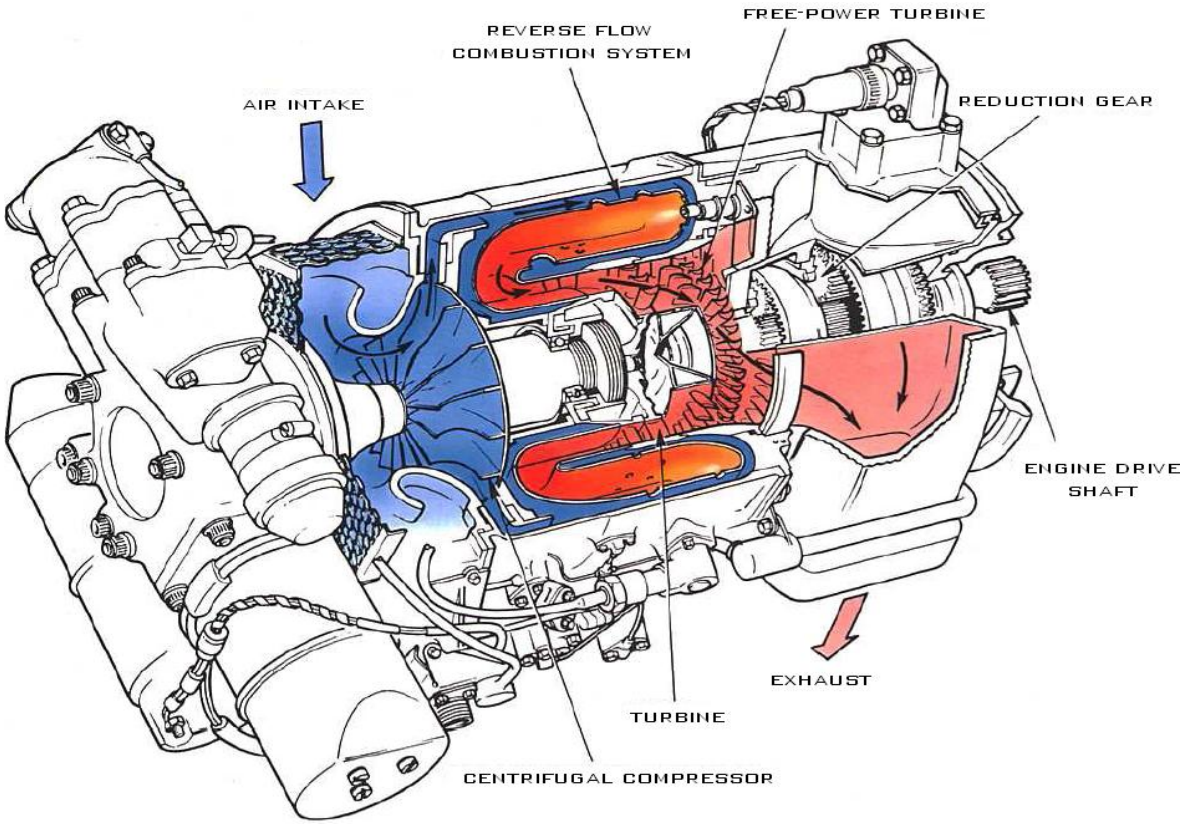

compressor, as compared to an axial-centrifugal type, has significant advantages in terms of pressure ratio and mechanical simplicity. In case of combustion chamber, a reverse flow annular configuration is preferred for its advantages over other straight flow combustors. It minimises the engine length, provides good accessibility to fuel nozzles and allows for a short and rigid gas generator rotor. Also, it allows a close coupling between centrifugal compressor and high pressure turbine design.Therefore, like most of the small gas turbine engines, the APUs have a centrifugal compressor followed by

reverse flow combustor, power turbine or GGT that drives the compressor and a free power turbine that powers the hydraulic/electrical systems and exhaust system. The working fluid is compressed in the compressor, heated in the combustion chamber and then expanded in the power turbine, thus producing power.

Figure 1.2 shows the picture of a typical Gas Turbine Starter (GTS). The architecture of GTS is very similar to that of APU.

Choice of the type of turbine in the gas turbine design depends on various factors like specific speed, number of stages, space availability, thermal/structural integrity and manufacturing feasibility. In the present thesis, the prominence is given on single stage axial turbine design. A turbine stage, in general, is composed of a row of stator blades followed by a row of rotor blades. The number of stages however depends on many factors dictated by the application and design requirements of the engine.

1.2 Turbine Design Methodology

The performance of a gas turbine engine depends on almost all the individual component performances like the compressor, combustor, turbine, etc. Since the turbine has to power the compressor, turbine design should incorporate a very minimal loss. The performance enhancement of a turbine stage is achieved mainly by increasing both the overall efficiency and the specific power, hence reducing the SFC considerably. Further, in order to design a high performance turbine, it is necessary for t

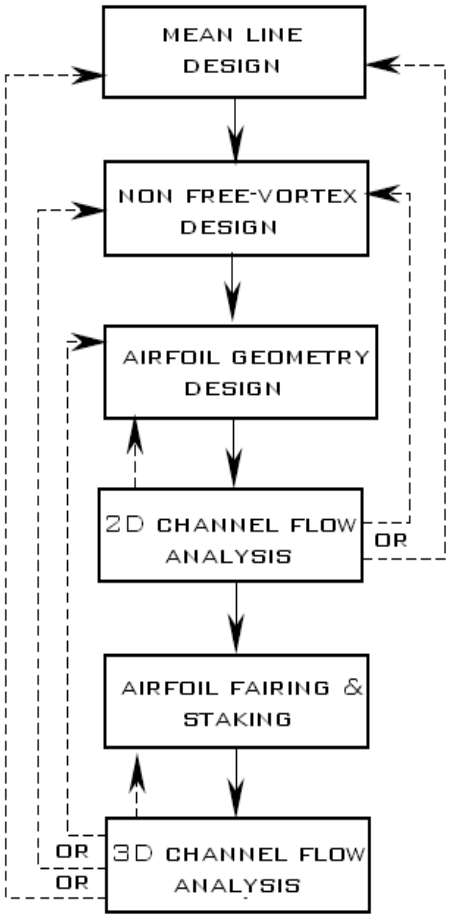

Figure 1.3 Turbine Design Process [1]

of off-design operating conditions other than the design point.

The turbine design process can be broadly classified as preliminary design and detail design process. A flow chart of turbine design process is shown in the Figure 1.3 and each step in this turbine design process abides a number of correlation.

Correlations are used to predict the efficiency of the turbine and thus the SFC of the engine.

They are also useful in evaluating the behaviour of a gas turbine engine under varying conditions. They assist in predicting aerodynamic losses and in understanding the effect of design changes and off design conditions on the efficiency of the power plant. Such correlations are needed at all stages of the design of turbomachines. While CFD is displacing such methods in the 3-D aerodynamic design of components, the fact is that correlations will still be needed for a long time to come for the 1-D mean line and 2-D through-flow preliminary analyses of turbomachines. Such 1-D and 2-D design steps are essential features of the overall design process of a turbomachine.

Development of these correlations requires extensive experiments. If carried out on actual engines, this would be a very expensive operation. Thus, most test data, used for formulating these correlations, are obtained from cascade experiments. Unfortunately, the cascade predictions are not free from experimental errors, and they apply to 2D cases rather than to the actual 3D turbines, since the flow in a turbine is much more complex than in a cascade. The real situation is one of three-dimensional flow, high radial pressure gradients, centrifugal and Coriolis forces, and high turbulence levels.

Thus the necessity of using less expensive and more complete tools to get good correlations is very important. One of the powerful tools that could replace experiments at much lower cost is through CFD. The fact is becoming truer with time due to the significant progress and affordability of computational tools. However, CFD has its own sources of error that should not be ignored. Its accuracy is dependent on the governing equations and the way the boundary conditions are applied in the modelling.

The thesis “Design and Analyses of a Free Power Turbine for an Auxiliary Power Unit” is clustered into seven chapters. The second chapter deals with literature survey to appreciate the

progress in technology of small gas turbine design so far. The third chapter defines the current problem of the thesis, whereas, fourth and fifth chapters describe the approach of preliminary and detailed design of the turbine. In the sixth and seventh chapter, results and discussions of computations are dealt with conclusions.

2 – Literature Review

2.1 Introduction

A wealth of experimental data on turbines has been generated in the literature to explore new design concepts and improve the physical understanding of design principles, methodologies and limitations imposed in the design of gas turbine engines. Especially in the field of small gas turbine engine design, many correlations have been developed from cascades, rig testing and design experiences. Emphasis is now given on the numerical techniques to simulate these correlations and to generate the test cases for CFD validation. This chapter gives a review of a small portion of the very vast literature that is published in connection with the small gas turbines.

2.2 Technological Requirements for Small Gas Turbines

The desire to achieve higher performance of small gas turbines expects special attention towards the application of technologies for components and structural sections thereby accommodating desired thermodynamic and aero-structural loading conditions.

Small advanced technology gas turbine engines have a target of high specific power, low SFC and improved power to weight ratio. Therefore a smallest possible engine needs to be designed. High pressure ratios, in addition, would lead to smaller dimensions of the hot section. Though these small engines cope with the requirements of mass and envelope constraints, they suffer from the adverse effect of scale. Spirkl's [3] work has deliberated upon a designer's view of engine requirements and has discussed the procedures of addressing these issues. Also included were design philosophies for meeting expected life requirements and designing for future. The approach appeared to be consistent with the requirements adopted by procuring agencies of the NATO countries.

Calantuoni et al [4] highlighted the trend to improve engine performance through turbine inlet temperature and indicated the need for advanced materials, technologies and sophisticated aerodynamic design methods, based on CFD tools to achieve improved component design at

reduced development costs. In addition they highlighted the need for further increase in stage aerodynamic loading ($\Delta H/U^2$) and work capacity ($\Delta H/T$) levels.

Substantiating the technological growth in small gas turbines and in the field of APUs, Hirtz and Mischel [5] have described various models of APUs and their special application requirements, ranging from shaft output to air delivery systems and hybrids of them at sizes up to the equivalent of about 260 kW. They have also focused on the technologies needed, and those available, to be adopted in meeting the future demands of the user in terms of 30% lower fuel consumption, lighter weight, and reduced cost of ownership. In that context, it was expected that the next generation of these units will have pressure ratios in excess of 7:1, operating temperatures increased by 70°C and operating lives competitive with the larger engines. The views of Hirtz and Mischel [5] have also been supported by Silet [6] and Vinic et al [7] based on their field experiences. Special attention was given by them to explore the other emerging requirements like starting envelope, lower noise level, full containment in the event of the disc burst, operating temperature, weight reduction, vehicle space limitation, degree of modularity and the challenge of meeting the cost targets.

Also, at the modular and component level, major works have progressed. However, focusing our attention towards turbine design, Dietrich et al [8] have reported that the reduced number of turbine stages is one of the key features in the advanced small engine design. A single stage, as compared to two stages, gives the best solution not only in reducing the weight and cost, but also in increasing the turbine aerodynamic loading, giving a good efficiency level without affecting the engine performance.

2.3 Architecture of Small Gas turbine

While engine architecture will vary between engines, a common concern is the large ratio of internal surface area to volume, forcing unique solutions to geometric problems.

Silet [6], in his work, has discussed a family of auxiliary power units available for use in a variety of aircraft applications and has furnished a pictorial way of selecting the architecture for a given engine rating. On the other hand, Calantuoni et al [4] have stressed more upon selecting a compact configuration, thereby reducing the production and maintenance costs, as well as the weight. The new architecture required reduced number of components but faced

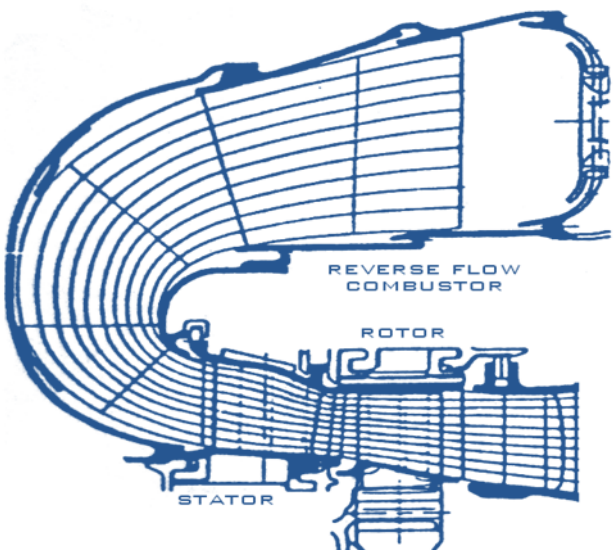

Figure 2.1 Turbine Architecture [3]

severe constraints on the overall geometry, like short axial length and reduced diameter that could be negotiated by an optimised design. As a supportive effort to this concept, a similar approach was also incorporated in the MTR390 engines [3], which have very compact dimensions and similar core configuration: Centrifugal compressor, reverse flow annular combustor and a gas generator turbine.

3] to describe the process of selecting an engine configuration and the arrangement of the aerodynamic components. Refined analytical design methods and rig test results rendered possible a significant progress in turbine aerodynamics. This, in combination with the availability of improved materials, paved the way for a change from the traditional two stage turbine to a single stage design. The aerodynamic design of the turbine, which included the inter-turbine duct, is shown in Figure 2.1. Similar architecture and perception have been incorporated in our concept.

2.4 Design Concepts and Requirements

The quest for an optimal concept in the design process of small gas turbine engines is absolutely a challenging task as the process of design is highly interdependent and non linear. It embraces various disciplines of engineering and hence effective compromises have to be made to satisfy all the involved disciplines by developing concurrency.

2.4.1 Performance Criteria

For single stage high pressure ratio turbines, most of the analyses carried out in the past, have also been carried out experimentally. Calantuoni [4] has discussed the design of a highly loaded $\Delta H/U^2 = 2.14$ turbine for an expansion ratio of 2.7 for developing 1000 kW of power. The design involved a mass flow of function $W\sqrt{T}/P = 15.6$, turbine inlet temperature of 1600 K, work capacity $\Delta H/T = 210$, flow coefficient $V/U = 0.65$, blade speed function $U/\sqrt{T} = 909$ and

rotor hub tip diameter ratio of 0.8. The higher power output was mainly due to the use of cooled turbine blades and the consequent higher TIT.

For the preliminary design, the loss estimation of the NGV and the rotor blade rows was done based on the experimental cascade data. The nozzle had 23 vanes of aspect ratio 0.58, a turning angle of 71 deg and an exit Mach number of 0.89 at the vane mid section. The rotor had 27 blades of aspect ratio 0.83, a turning angle of 114 deg and an exit Mach number of 1.06. A total to total efficiency of 88 %, excluding windage and bearing losses, was predicted with a tip clearance ratio of 2%.

A similar kind of study was done by Trazzi [9] on the performance of a lightly loaded $\Delta H/U^2 = 1.1$, single stage, axial turbine, whose tip diameter was restricted to 56 mm and the axial width was 6 mm. The 29 number of rotor blades were accounted in the design with an axial solidity of 1.1 at the mean diameter. The requirement of the turbojet engine was to develop 74 N of thrust with a mass flow rate of 0.155 kg/s. The flow factor assumed here was 0.7. However, the performance parameters, when examined at static sea level condition, gave the required thrust of 74 N for a specific fuel consumption of 1.45 kg/daN/h and a total to total turbine efficiency of 0.80.

Perhaps the most recent work on the performance analyses of a highly loaded single stage turbine is reported by Schaub et al [10]. They reported the aerodynamic design of a turbine stage with a pressure ratio of 3.75 and an aerodynamic loading $\Delta H/U^2 = 2.47$. The other design parameters included an inlet total temperature of 400K, mass flow rate of 4.38 kg/s, flow coefficient of 0.64, work capacity of 265 J/kg/k and a blade speed function $U/\sqrt{T} = 1.3$ for a rotational speed of 8852 rpm.

As an in-service example, the auxiliary power unit TGA-15 of Turbomech [6], which is used to start many fighter aircrafts like Rafale and Grippen, has the gas generator operating at 47500 rpm with a mass flow rate of 2.16 kg/s. The power output is around 245 kW, which is used either to drive the load compressor or start the main engine. Also, for the Fiat Avio APUs [7] the rotational speed of the turbine is 54500 rpm. The other design features include an external diameter of 250 mm, approximate overall pressure ratio of 4 and a stage efficiency of 0.78. In

fact, these specifications are very close to the ones used in the current design. 2.4.2 Aerofoil Design Criteria

Blade designs have to conform to the velocity or pressure distribution along their surfaces so as to meet the efficiency requirements. This can be achieved only by controlled design of the aerofoil. Some of the techniques are discussed here:

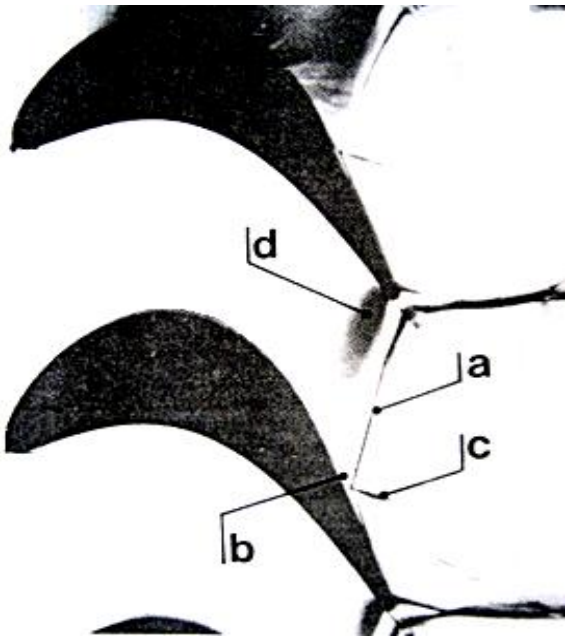

Figure 2.2 Turbine Aerodynamics [8]

2.4.2.1 Influence of Transonic Mach Number on Stage Design

Dietrichs [8] has discussed the design and development of a single stage turbine for the gas producer section of a modern small engine in the 1000 kW class. Because of the high stage loading and the accompanying transonic conditions, initial emphasis in the design phase was directed at cascade tests. The steps taken to select the rotor airfoils best suited to accommodate transonic exit Mach number of 0.9 to 1.2 were discussed. The e of the areas at airfoil choking conditions were also illustrated.

It was observed that the aerofoil design was strongly influenced by the small dimensions of the vanes and blades. For a chord length of about 19 mm and a trailing edge thickness of 0.5 mm, a trailing edge wedge angle of 6.5 degrees was required. For a larger blade, due to bigger overall dimensions, a smaller wedge angle of about 3 degrees would be acceptable. The flow field on the suction side of a transonic turbine blade is highly influenced by the pressure side geometry. The increase of the pressure side trailing edge wedge angle led to a considerable increase of the suction side peak Mach number with consequently higher shock losses.

Figure 2.2 shows the Schlieren picture of a transonic rotor blade at an exit Mach number of 1.25 with all the main transonic flow phenomena, which control the aerofoil's loss mechanism, like trailing edge compression shocks (a), separation bubble (b) and expansion waves (c) and (d) respectively.

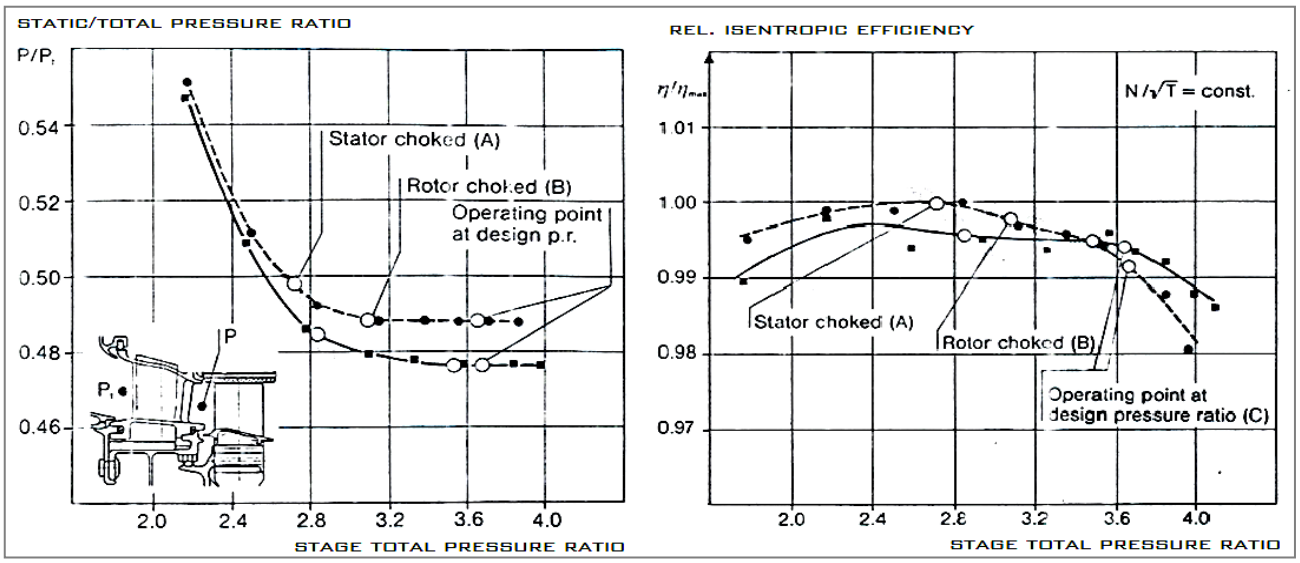

(a) (b)

2.4.2.2 Rotor Stator Matching Effects

Dietrichs [8] also highlighted the significance of choking in both rotor and stator blades. It was concluded from his analyses that for a highly loaded single stage turbine, the exit Mach number levels for both rotor and stator depended on the stage pressure ratio and the relative size of the throat areas. Normally higher stage pressure ratios would lead to choking.

The choking process and its influence on the stage efficiency of a transonic turbine can be seen in Figure 2.3 (a) and (b) for two different vane flow capacities. The choking condition of the vane is (A) and that of the rotor is (B). This example from Dietrichs [8] shows the importance of careful control of the aerofoil loss characteristic as well as of the vane and blade area matching.

Figure 2.5 (a) Static Pressure Characteristic and (b) Efficiency Characteristics of a Transonic Turbine Stage [8]

2.4.3 Structural Design Consideration

The components, whose failure would yield high energy fragments and which are unlikely to be contained by the engine castings, are classified as fracture critical parts. The FA 150 [7] gas generator spool components were considered as fracture critical parts. This necessitated safe life criteria to be assessed for low cycle fatigue under appropriate stress, temperature conditions, High Cycle Fatigue, over speed failure and creep failure. Such an APU is designed for a fatigue life of 4000 cycles and the burst pressure is 75 % over the starter power unit.

The turbine blade speed as well as the choice of the turbine annulus has been constrained by the consideration of the blade and disc stresses, in order to maximize the engine life. This can also be attributed to the material limitations.

Apart from this, the importance was also given to vibrations, resonant frequencies, and oxidation/corrosion phenomenon.

2.4.4 Thermal Design Criteria

Although the combustor liners, nozzle guide vanes and the rotor blades of the turbine are exposed to hot gases, the rotor blades can be considered as the most critical component since these blades solely contribute to the shaft work. Also, rotation of the blades makes them difficult to cool. Experts opine that the blade life may reduce by half if the blade metal temperature prediction is off by only 300° C. These factors necessitate the cooling of blades. But in the case of small gas turbines it is highly difficult to produce the blades with very small cooling holes. Therefore small gas turbines usually are un-cooled type

The work of Vinci [7] dealt with the development of an APU for a fighter aircraft which has un-cooled blades. Similarly Fiat Avio [7] has un-cooled blades as it was not practical to cool the blades with such small components for 200 HP range power engines. The same technology is used in the current design with a concurrency in material selection.

2.4.5 Machining Consideration

Integral cast rotors are called as blisks. These have basically un-cooled blades leading to obvious advantages in terms of manufacturing feasibility, and consequently cost savings and

giving more freedom on profile design (i.e., thinner blades). The use of blisks also reduces the cost. The only problem with the blisk is its very high response to excitation and therefore is susceptible to HCF failure [7]. Also, it should be noted that the aerodynamic design optimisation of a transonic aerofoil for exit Mach number of 1.1 for a small engine is significantly restricted by casting and manufacturing limitations [8].

2.5 Loss Modeling

In the last 50 years, many turbine correlations have been developed, based on the data obtained from cascades and rig tests. Most of these methods focused mostly on design point conditions. Probably the most complete and comprehensive method of predicting the design and off design performance of axial turbines is that due to Ainley and Mathieson [12]. Later, several improvements to the Ainley and Mathieson correlations were made considering profile, secondary and tip clearance losses at design and off-design conditions.

2.5.1 Pressure Loss in Blade Rows

The pressure loss in the blade rows is subdivided into four components, namely profile loss, secondary loss, tip or shroud clearance loss and annulus loss. The profile loss is due to the skin friction or flow separation, due to two dimensional flows across a cascade of blades. The secondary loss is a result of non uniformity of the three dimensional flow through a row of blades or, in particular, the losses due to the interaction between the blade ends and the boundary layer on the annulus walls. The tip clearance loss is due to the leakage of gas around shroud bands, and lastly the annulus loss is due to the skin friction loss on the end walls of the row of blades.

Ainley and Mathieson [12, 13] method has been used for many years in turbine performance predictions. This method is based on several broad assumptions and a correlation based on the compiled data is available to calculate the blade losses. The method can be used to predict the performance of an axial flow turbine with conventional blades over a wide part of its full operating range.

2.5.2 Profile Loss

Ainley and Mathieson [13] gave a profile loss model based on the experimental data from on a variety of turbine stages. These blade profiles were designed prior to 1955 and had either

blade profiles with contours composed of circular arcs and straight lines or blades which made use of the British blade profile series with circular or parabolic camber lines. The maximum blade thickness considered was between *t/c* = 0.15 to 0.25. The correlation was based on a series of graphs of total pressure loss versus *s/c* ratio for nozzle and impulse blades. Figure 2.4 and 2.5 shows profile loss coefficients for conventional nozzle and impulse blade sections composed of RAF 27 section on circular arc and parabolic camber lines. This data is valid for a trailing edge thickness to blade space ratio of 0.02, Reynolds number of $2x10^5$ and Mach number less than 0.6. For the blades that are intermediate between nozzles and impulse blades may be interpolated using the equation (2.1).

$$Y_p \approx \left[Y_{p(\alpha_1=0)} + \left(\frac{\alpha_1}{\beta_2} \right) \left(Y_{p(\alpha_1=\beta_2)} - Y_{p(\alpha_1=0)} \right) \right] \left(\frac{t/c}{0.2} \right) \quad \ldots\ldots (2.1)$$

To calculate the profile loss at incidences other than zero, it is necessary to evaluate the stalling incidence, i_s and employ the relationship with $Y_p / Y_{p(i=0)}$

2.5.3 Secondary Losses

The basic equation for secondary loss coefficient, given by Ainley and Mathieson [12], was derived from performance measurements on conventional blades using the correlation already established for profile losses. The loss is calculated based on the blade loading, which is considered as a main function of the blade turning. The secondary loss coefficient can be calculated using the correlation (2.2)

$$C_{DS} \approx \left[C_l^2 / s/c \right] (\lambda) \quad \ldots\ldots (2.2)$$

Where λ is a parameter which is function of the flow acceleration through the blade row

$$C_l / s/c \approx 2 \left[\tan\alpha_0 - \tan\alpha_1 \right] (\cos\alpha) \quad \ldots\ldots \ldots\ldots\ldots\ldots (2.3)$$

$$\alpha_m = \tan^{-1} \left[(\tan\alpha_0 - \tan\alpha_1)/2 \right] \quad \ldots\ldots (2.4)$$

Then finally, the secondary loss can be calculated by the equation (2.5)

$$\lambda [C_l / s / c]^2 [Cos\alpha_1 / Cos\alpha_m] \quad \ldots\ldots (2.5)$$

Perhaps the most recent work by Sauer and wolf [14] has addressed the end wall losses as influenced by the inlet boundary layer and also the current inaccuracies in predicting the downstream effects. Potential approaches to aid in reducing the loss effects pointed towards better optimisation of axial gaps between the cascade rows and a need for improved turbulence modelling. An example to illustrate the tip leakage effects was presented for a blade of 30 mm height for shrouded and un-shrouded turbines. The higher thermodynamic efficiency was attributed primarily to the avoidance of tip vortex over a large portion of the blade, accompanied by less deviation of the flow.

For small blade heights, the secondary loss constitutes a great portion of the overall cascade loss, and therefore, the efficiency level is mainly determined by the secondary losses. The other parameters which influence the secondary losses are aspect ratio, chord length, thickness aerodynamic loading, and roughness of the endwall, Mach number levels and special shape of the inlet boundary layer.

2.5.4 Tip Clearance Losses

As the tip clearance in the blade row of a turbine is increased, the pressure losses increase, resulting in a decrease of turbine efficiency. A non-dimensional empirical formula was developed by Stodola, as reported by Ainley and Mathieson [12, 13] for the loss associated with tip clearance, which is given by,

$$\zeta_{clearance} = 6.26k^{1.4} / h, \quad \ldots\ldots (2.6)$$

Equation (2.6) was still not regarded satisfactory.

However, the most recent work by Schaub et al [10] concentrated on quantifying the tip clearance losses for a specific turbine designed to operate at transonic conditions with high stage loading and a pressure ratio of 3.75:1. Experimental hardware was roughly three times the full size. The mean radius of the tested turbine stage was 229 mm and blade height was about 75 mm. Two configurations were tested; one with 51 rotor blades and the other with 34 blades, both with 14 nozzle guide vanes. The mean reaction was about 30%. Analysis of test data showed the

influence of the tip clearance on generating a strong vortex that extended over much of the blade span. For a nominal clearance of 1.5%, the changes in flow turning caused a penalty in the efficiency of 1.1% at part-speed and 2.6% at full-speed. In addition, reducing the rotor speed also had the

blades and the other with 34 blades, both with 14 nozzle guide vanes. The mean reaction was about 30%. Analysis of test data showed the influence of the tip clearance on generating a

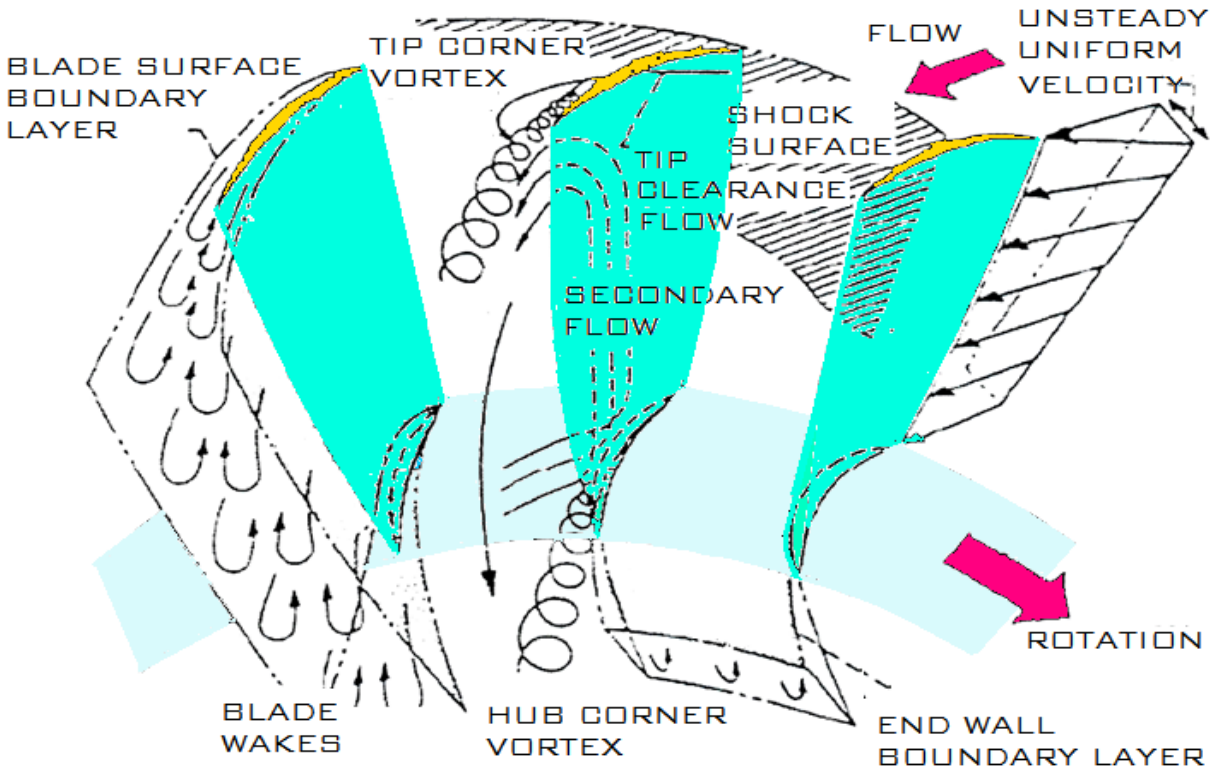

strong vortex that extended over much of the blade span. For a nominal clearance of 1.5%, the changes in flow turning caused a penalty in the efficiency of 1.1% at part-speed and 2.6% at full-speed. In addition, reducing the rotor speed also had the effect of increasing the exit swirl, as might be expected for off peak operation, resulting in lowering the efficiency by about 9 %. Reducing the blade number caused under-turning of flow and a lowering of the efficiency by 4 %. It was concluded that the effects on the efficiency due to small clearance changes (1.5 % to 2.1 % of blade height) were overshadowed by changes in the loading brought about by the 51 and 34 bladed rotors. Similar views on the tip clearance were also supported by Dietrichs [8] as he demonstrated an analysis to show the influence of tip clearance variations on performance.

Figure 2.6 Flow Structure in the Turbine cascade showing Boundary Layer Growth, Tip Clearance Flow, End Wall, Secondary Flow and Blade Wakes [17]

The total pressure loss in a turbine cascade by Ainley and Mathieson [12] consist of profile loss, secondary losses, tip leakage loss given by equation (2.7).

$$\boxed{Y = Y_S + Y_K + Y_P} \quad \ldots\ldots (2.7)$$

A typical flow structure in the turbine cascade associated with various flows mechanisms is shown in the Figure 2.6. Each flow mechanism has loss associated with it.

2.6 Advanced Materials for Small Gas Turbines

Small gas turbines invariably operate at very high speeds, as a result of which hot section rotating components such as turbine blades and discs are subjected to high centrifugal loads. High centrifugal stresses coupled with high operating temperatures make blades and discs prone to creep. Therefore the load bearing capacity at higher operating temperatures is a highly challenging task. Moreover, the cooling of these miniature components is also not feasible because of its small size. Hence the advancement in the material technology is necessary. A chart, useful for identifying materials for components which operate at various temperatures above room temperature is shown in Appendix-A.

Table 2-1 Basic Materials and Thrust Data on Small Gas Turbines [15]

APPLICATION / TURBINE IDENTIFICATION	THRUST OR HP	RPM	TIT °C	VANE MATERIA	BLADE MATERIAL	DISC MATERIA
CRUISE MISSILE/F17 WR 100 CRUISE MISSILE	2.67 kN	64000	954	Integrally cast IN100 Wheels		
EUROLIGHTER / BMW-RR T118	196 kW	47000	1002	Integrally cast Mar M 247 LC Wheels+HIPed		
FH1100 BELL 206A 369 H / AGT 250/T63-A700B C-18	236 kW	35000	749	HS31 (uncoated)	Integrally cast Mar M 246LC Wheels+HIPed	
CITATIONS CORVETTE, AUGUSTA T21, BEACH JET, T47-A / PWC JT15D	9.8/12.9 kN	31800	988	IN792	DS Mar M 200	Waspaloy
FALCON /GT-TFE731-2-1C	14.4 kN	29692	865	Mar M 247	Mar M 247	Astroloy
EH101/ GE T700/CT7-6/6A	1491 kN	20,900	950	Mar M509	DSR 142	Rene 95
F-18 / GE F404-400	11931 kW	14000	1100	MA754	DSR 80	Alloy 718

Koul [15] has presented a review of the material used in hot sections of small gas turbine engines. Special attention was given to the unique aspects of small engines that permit the use of integrally cast blisks. It was also shown that the expanding base of the material technology development will lead to wider use of dual property discs, new powder metallurgy discs, new generations of directionally solidified and single crystal super alloys for blades, and Thermal Barrier Coatings.

Koul [15] addressed the basic materials and temperature data for some small gas turbines, as tabulated in Table 2.1. The material that is highlighted in the table is considered for the current design of axial turbine.

2.7 Summary of the Literature Review

From the wealth of experimental and computational data on turbines gathered through literature review, the following points are summarized.

- For a 315 KW range of gas turbines, the turbine architecture consisted of a single stage axial turbine for the Gas Generator Turbine (GGT) and most of them were running at the speeds greater than 35,000 rpm.
- All the high performance engines implemented higher turbine inlet temperatures, higher blade reaction, blade loading and lower exit swirl angles in the design.
- Most of the small gas turbines and APUs were un-cooled type.
- Designs based on modularity, manufacturing feasibility and structural integrity were also given wide scope in terms of trade-offs.
- H-O-H type of grid was mostly used in the analyses of high pressure turbines.

Mechanical design incorporated design for 15% over speed to overcome burst margin

2.8 PROBLEM STATEMENT

Small gas turbines have gone through enormous changes since their first appearance in the 50s. The evolution of the small gas turbines has been primarily driven by the influence of military requirements as there was a need of something better than piston engines.

Developments in the core engine to achieve higher operating pressures and temperatures have led to smaller and lighter engines. The matter of fact now is to appreciate new concepts and processes that give unique solutions to the lower life cycle cost and higher life of the components without deteriorating their performance. The new technologies developed under the Integrated High Performance Turbine Engine Technologies (IHPTET) addresses the need for new materials and component technologies to achieve these targets.

As an encouraging consequence, implementation of computational tools in the field of turbo-machinery is also continually improving. Tools for Computational Fluid Dynamics (CFD) simulations and Finite Element Methods (FEM) can now perform virtual simulations and hence are becoming the regular tools for design and analysis. Particularly, when testing is an alternative, computational codes are the best choices as they have the potential to reduce overall

cost and time. The current design requirement for an axial turbine stage is based upon a potential future application in a high performance small turbo-shaft engine (APU). The primary objective here is to design an un-cooled turbine stage having maximum aerodynamic performance while operating within the limits of aerodynamic and mechanical constraints.

2.9 Problem Statement

To design and carry out aerodynamic and structural analyses of a single stage high performance gas turbine for an auxiliary power unit of a multi-role combat aircraft

2.10 Objectives

- To review the literatures and MIL standards on turbines for small gas turbines and Auxiliary power systems
- To perform preliminary design based on correlations
- To generate three dimensional model of the designed turbine stage
- To carry out the grid generation, Computational Fluid Dynamic (CFD) analyses and compare the CFD results with the design targets.
- To perform parametric studies for improved performance characteristics of the turbine
- To select appropriate materials for blisk and stator vanes.
- To perform Finite Element Analyses (FEA) for disc optimisation.
- To compile and analyse the results and to generate report

2.11 Methodology

- Literature review on high performance turbines was carried out by referring MIL standards, refereed journals, books, manuals and related documents.
- The design specifications, dimensional constraints, modularity, and architecture of Auxiliary power unit (APU) were studied through specific requirements of military aircrafts
- A preliminary conceptual design was developed based on correlation, loss modeling and performance calculations at various operating range using Excel spreadsheet
- Blade profile generation and 3-D stacking of blade and vane were done in NUMECA software and the 3 D turbine blisk model was created in ANSYS Design Modeler 11.0

- Grid generation for CFD computations was carried out in NUMECA IGG Autogrid which is designed uniquely for turbo-machinery applications. Meshing for mechanical analysis was done in ANSYS simulation wizard.
- CFD analyses at design point, off design point performance analyses and parametric studies were carried out using FINE TURBO of NUMECA.
- Suitable materials were selected through weighted ranking method of material selection and experiences gained by ADA.
- Compilation and post processing for both aerodynamic and mechanical analyses was done in Excel spreadsheet.
- Final report of the thesis was documented in the MS word.

3 – Preliminary Design

The entire design process of axial turbine can be grouped as preliminary design and the detail design. The steps involved in primary and detail design are briefly described in the following sections.

3.1 Preliminary Design

Design of the axial turbine began with a one dimensional meanline preliminary design. A code was developed to execute the design iterations and keeping the maximum performance goal of the program, a number of design iterations were carried out. Unfortunately, the parameters that improved the aerodynamic performance, tended to degrade the mechanical integrity of the design and vice versa. A ‘design space’ was therefore generated considering the acceptable aerodynamic and mechanical bound limits, as shown in the Figure 3.1.

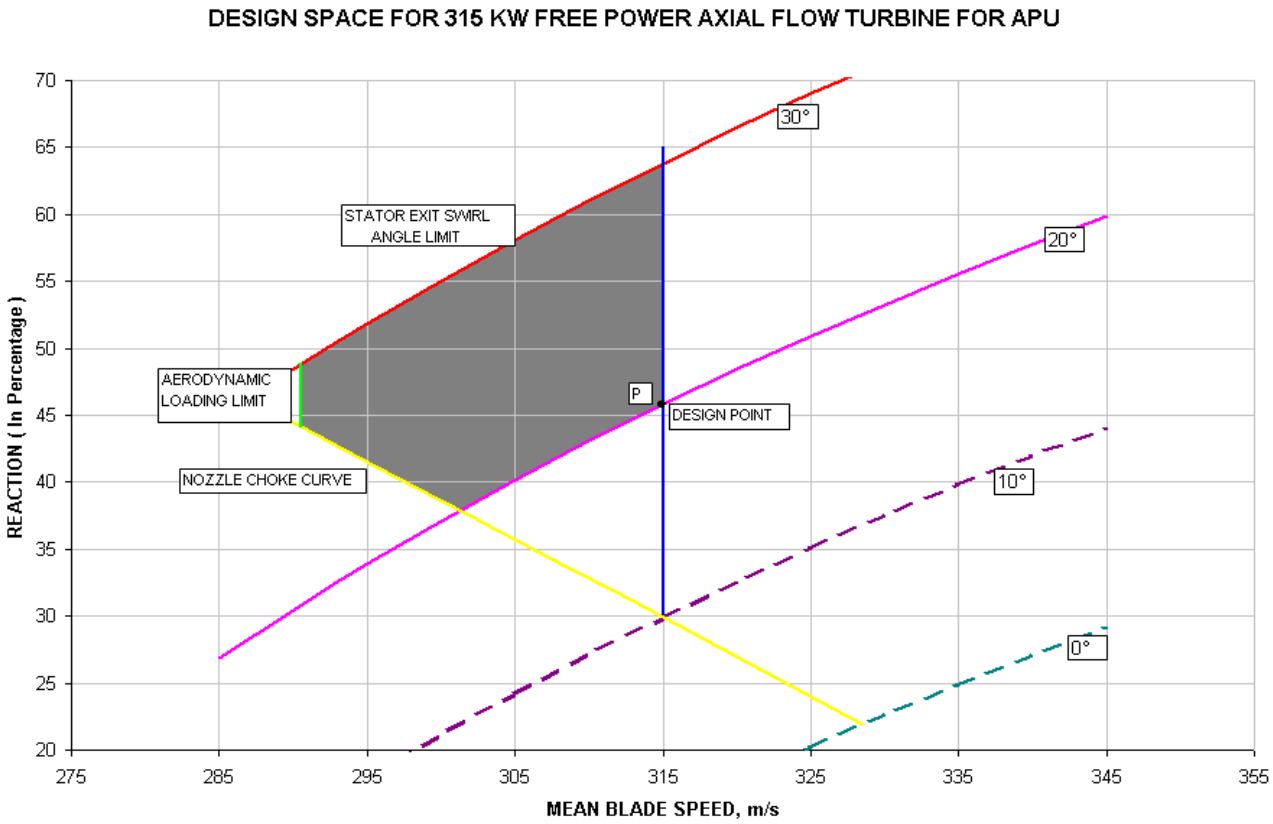

Figure 3.1 Design Space under Aeromechanical Constraints

From the design space, it can be observed that the designs in the lower left section of the acceptable region had the lowest mechanical risk in terms of tip speed, whereas designs in the upper right corner had the highest aerodynamic performance but with higher mechanical risks. Keeping the maximum performance goal, design point 'P' was chosen with a blade speed of 315 m/s and an exit swirl angle of 20°, which showed a reaction of 45.7%. Increasing the swirl angle beyond 20° caused problems for the downstream, where as further reducing the exit swirl angle, led to lower reaction. Increasing the mean blade speed beyond 315 m/s was not found feasible as far as the mechanical limitations were concerned. Here, the performance was measured in terms of efficiency and stage reaction, whereas the mechanical constraints were evaluated in terms of blade tip speed, disc stresses and vibration levels.

Some of the important steps that were necessary during the preliminary design process are summarized as follows:

3.1.1 Specific Speed and Architecture Selection

Specific speed is the parameter which determines the overall performance and the number of stages required for the turbine. The specific speed calculated to be 0.760 was close to the cut-off speed of 0.776 [16]. Figure 4.2 (a) shows the specific speed curves for axial and radial turbine stages. Though the calculated value of the specific speed for the axial turbine was on the lower side, the design was still chosen at that point to take the advantages of axial turbines over radial turbines in terms of overall diameter and weight.

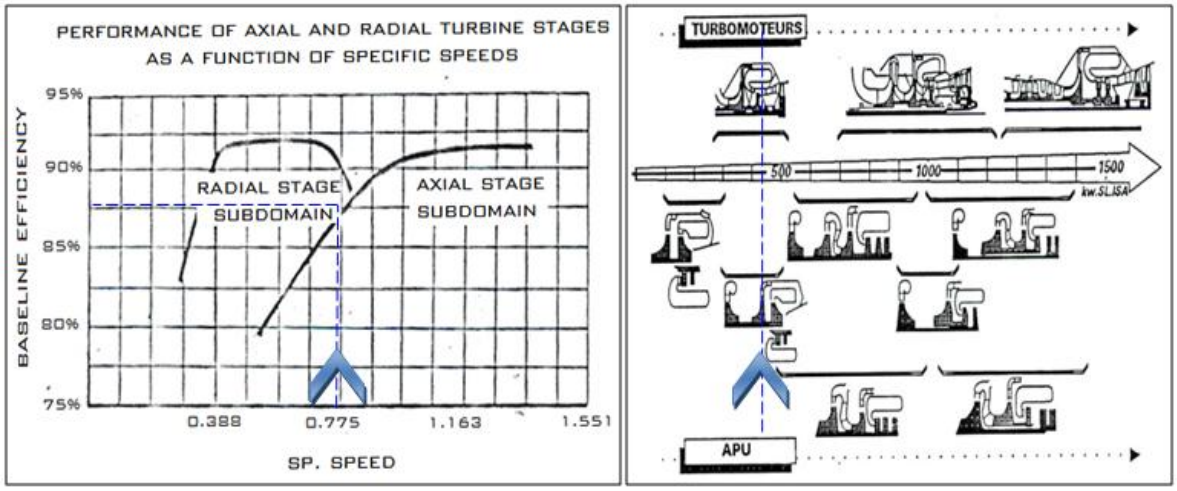

Figure 3.7 (a) Specific Speed Curves [16] and (b) Turbine Architecture Selection [6]

Though there were a wide variety of options in selecting the type of architecture for APUs, in the range of 315 kW of power, the one with single stage axial turbine was incorporated in the current design. This was to extract the advantages of axial turbine, over radial turbine, as discussed above. Figure 3.2 (b) shows the APU configuration for various power ranges and the dotted line indicates the architecture selected.

3.1.2 Stage Design

The highest expansion ratio practical from a single stage turbine with any acceptable level of efficiency is 4.5:1. However, the expansion ratio derived from the current

Blade aspect ratio: Chosen within 0.5 < 0.83 < 0.85 to minimize secondary losses

thermodynamic design was 2.05:1, which was well within the practical limits. Also referring to the 'design space', it can be noted that the design point chosen has the highest performance, which is a direct measure of the reaction. The highest reaction that could be achieved was 45.7% in the present design.

4.1.3 Rotor Tip Speed

The tip speed is a function of the rotational speed and is given by the formula,

Best efficiency: The pitch line reaction should be around 50% [16]

$$U_{tip} = \pi D_{tip} N / 60; \quad \ldots\ldots (4.1)$$

Where U_{tip} is the rotor tip speed in *m/s*, D_{tip} is tip diameter in *m*, *N* is the rotational speed.

Tip speed is the most important parameter that determines the blade reaction, choking condition and blade loading. It is observed that with higher blade speeds, higher performance can be achieved. But, because of higher operating temperature of 1000 K and material limitations, the blade tip speed also gets limited to 399 m/s. Mechanical limitations are also imposed in terms of the product AN^2 because of creep life limitations

3.1.4 Blade Height and Tip Diameter

Relatively high speed of the turbine rotor limited tip speed to 399 m/s. Therefore, it was calculated that a rotor of 140 mm was required for delivering a mass flow rate of 1.896 kg/s for a rotor speed of 43000 rpm. The inlet Mach number was taken as 0.4.

The rotor tip speed, tip diameter, mass flow rate and the cross sectional area were required to calculate the blade height, which was found to be 21 mm. This was in comparison with an MTU [8] turbine having a blade height of 17 mm.

3.2 Detail Design

Results obtained from one-dimensional mean line preliminary design were used as the basis for 2 D and 3 D detailed designs. The process involved in this phase of the design was non-linear since the steps involved were highly interdependent and embraced various disciplines. A number of iterations were necessary to obtain the final design.

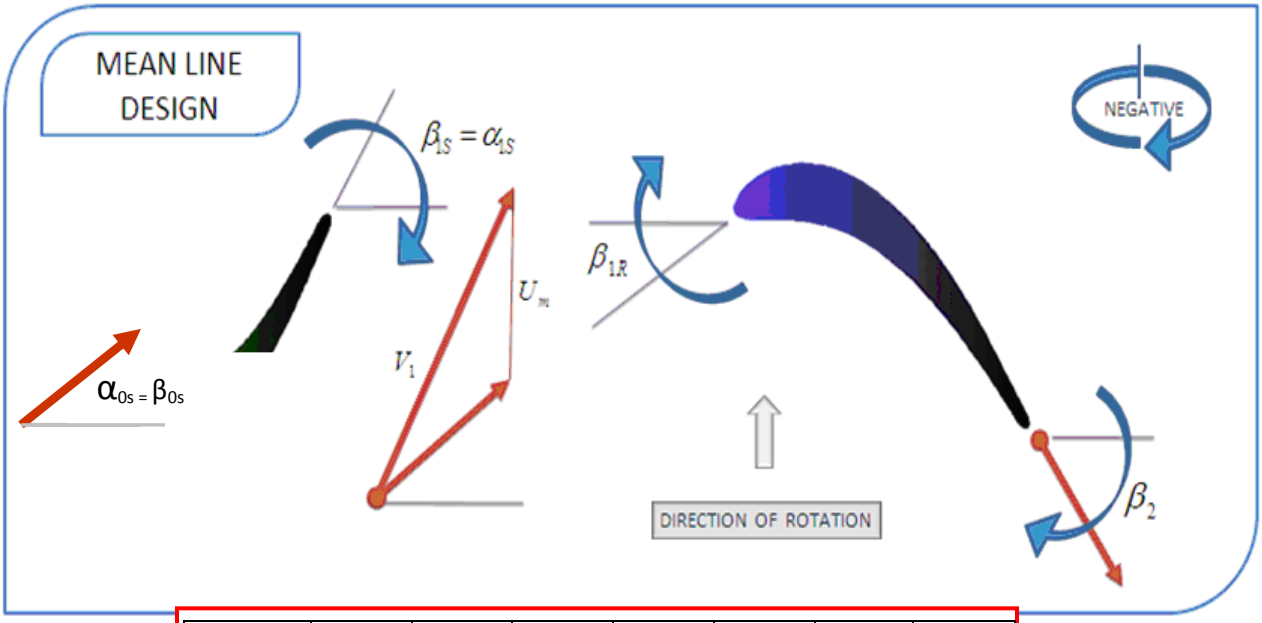

POSI-TION	$\alpha_1°$	$\beta_1°$	$\alpha_2°$	$\beta_2°$	U (m/s)	V_Z (m/s)	V_1 (m/s)
HUB	64.09	47.99	26.40	52.68	267.8	266	609
MEAN	58.78	25.02	20.00	57.13	315.0	266	513
TIP	54.01	-2.37	16.03	60.76	398.7	266	452

Figure 3.8 Velocity Triangles for Stator and Rotor Blades at Mean Line

To determine the blade angles, absolute angles and velocities at the rotor and stator ends, the velocity triangles were constructed and their magnitudes were measured using Auto CAD. Free vortex design was used to determine the velocities at hub and tip. Figure 3.3 shows the velocity triangle at mean line. The flow velocity and absolute velocity were found to be 266 m/s and 513.25 m/s respectively. Upon measurement of velocities and blade angles at mean, hub and tip, the blade profiles for the stator and the rotor were generated in NUMECA environment. These profiles were stacked radially to get 3-D blade models. A detailed account of blade

generation is given in Section 5.1.

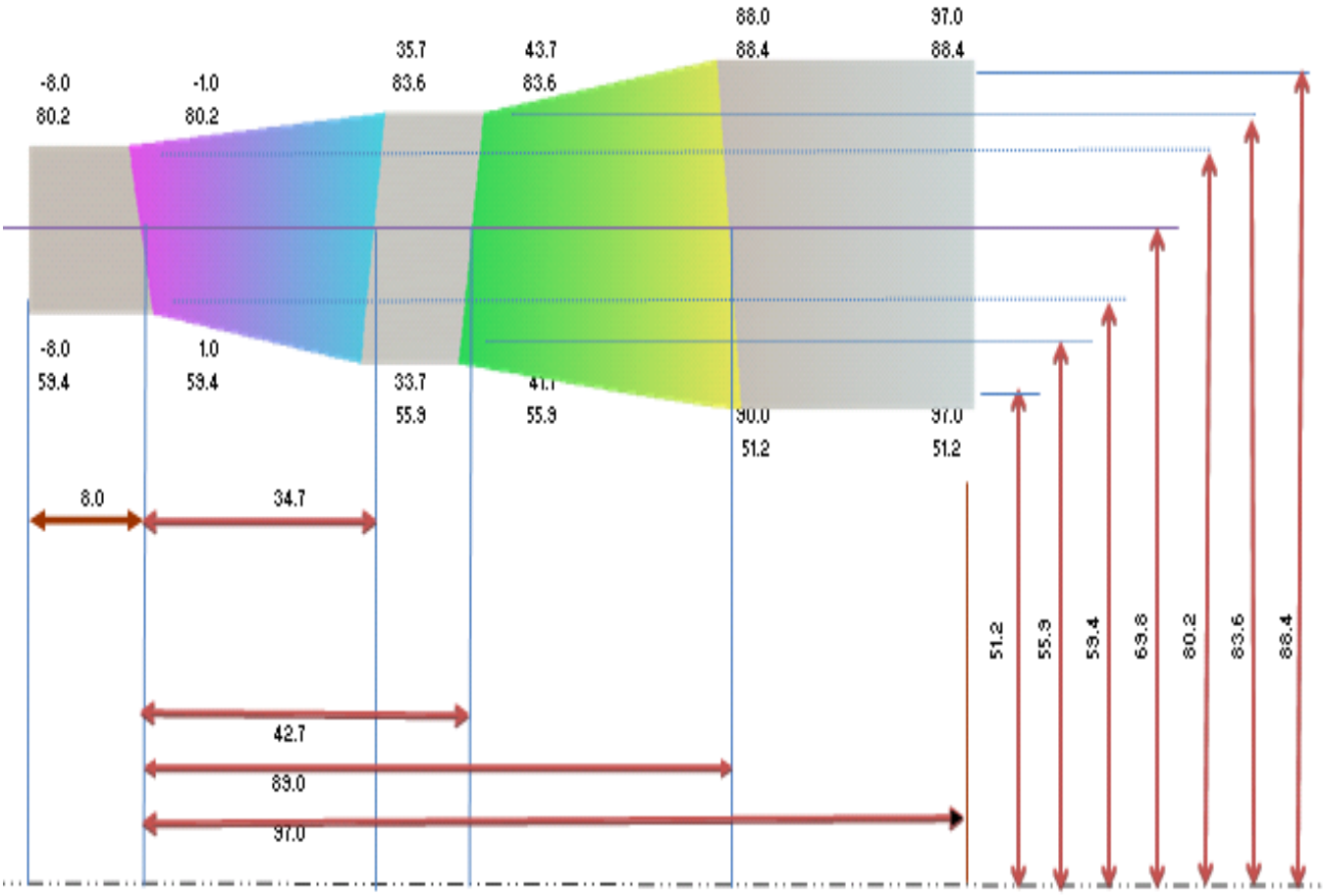

Figure 3.9 Automated Dimensioning System for Flow Path Generation

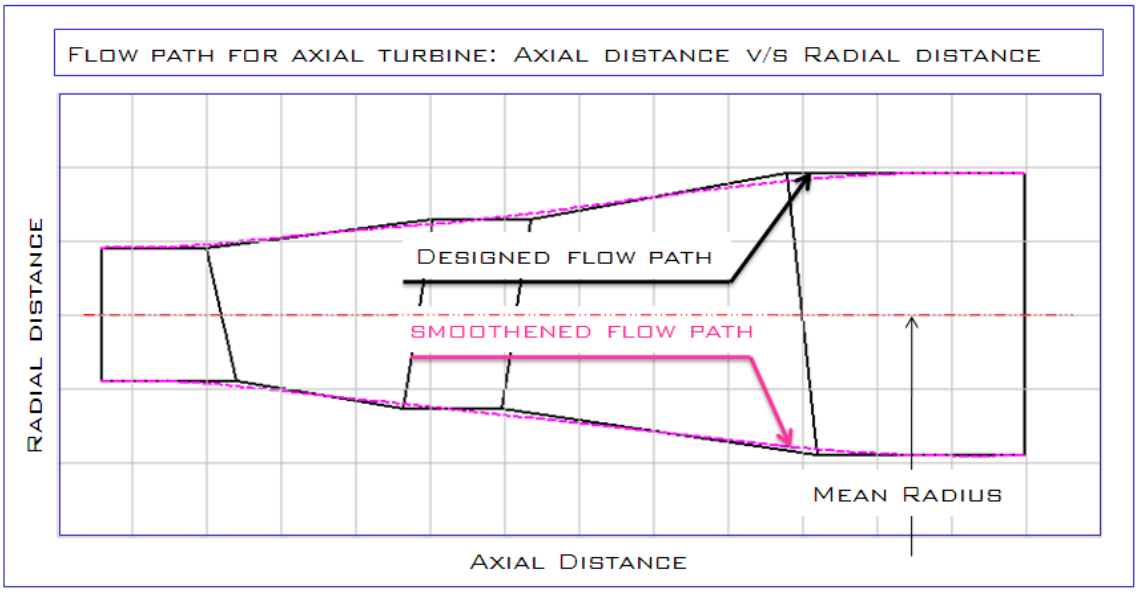

Figure 3.10 Designed and Improved Flow Path

Selecting the shape of the flow path is one of the critical step in detailed design phase as it not only defines the profile of the blade in the meridional view but also impacts on flow characteristics and the axial length. The axial length for instance was fixed as 4.75 mm, which was 25 % of upstream axial chord. Upon fixing the axial length, the incline angle was adjusted to smoothen the flow path, thereby improving the performance. In the process it was experienced that as the incline angle increased, the nozzle blades became too short making them difficult to manufacture. Figure 4.4 shows an automated normalized flow path dimensioning system wherein all the dimensions get updated with the change in preliminary design parameters and Figure 3.5 shows the meridional flow path for initial design and improved design of the stage. The designed flow path was simply based on the major dimensions that were computed in the preliminary design phase and the modified flow path was generated based on an approximation by fitting a 'spline curve' at the mid points of the blade rows and gaps.

3.3 Material Selection

High temperature, high strength materials and unique methods of manufacturing have made the aero engines a practical reality in few decades. When a more conscious study was made on the materials, and their applications, it was found that the nickel based alloys are mainly used in the hot sections of the engine as shown in Figure 3.6.

Conclusive remarks on material selection:

- Though hundreds of materials were available in nickel based material kingdom, only a few, such as Inconel, Nimonic, Waspaloy and Mar M 247 qualified as the material of turbine blisk. This was mainly because of the requirement of high strength, stiffness and toughness of the material at a very high temperature of 1200 K.
- Among the short listed materials, the other important criterions that were assessed are the creep resistance and corrosion resistance. However since in the preliminary design procedure, the product AN^2 was considered, it was confirmed that the material offers a very good creep resistance.
- Finally Mar M 247 qualified to be considered as the material of blisk.

In Figure 4.6, the blue colour indicates titanium material whereas red, saffron, yellow and green indicates nickel, steel, yellow and the composite materials respectively.

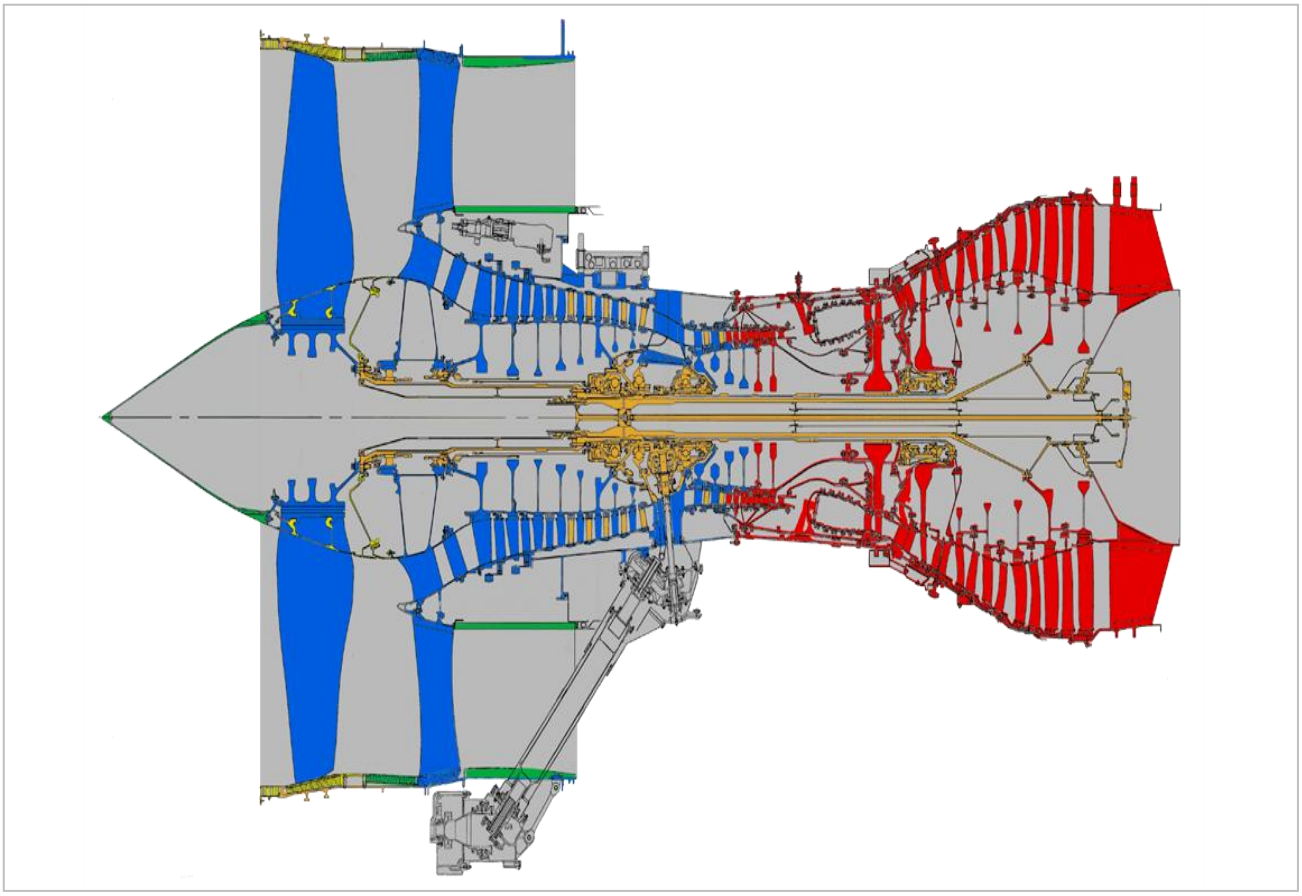

Figure 3.11 Material Distribution in Gas Turbine Engine [2]

3.4 Summary of Design Procedure

The overall design procedure of the present study can be summarised in a simple flow chart as shown in Figure 4.7. The flow chart also explains the multidisciplinary interactions' involved in the preliminary and detail design phase of turbine design.

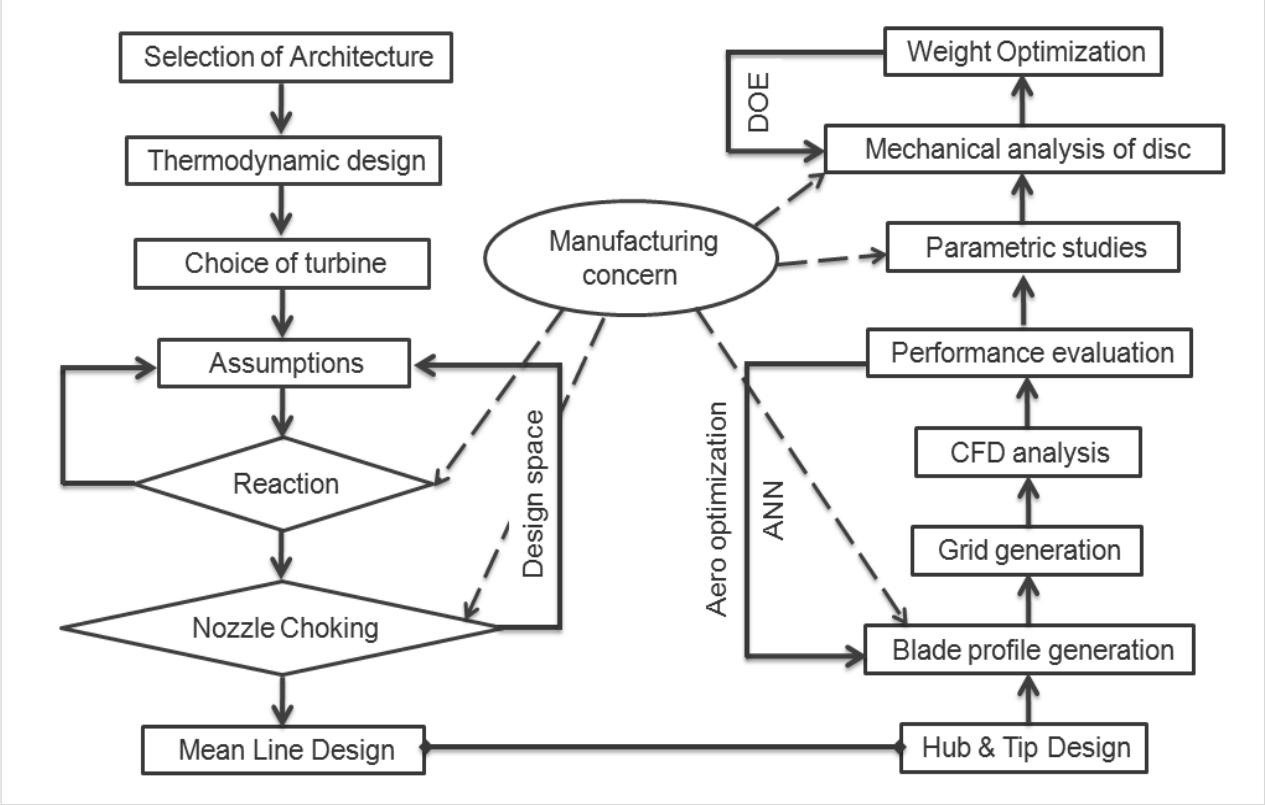

Figure 3.12 Chart of Turbine Design Procedure with Multidisciplinary Interaction

4 – Model Construction and Solution

The design of turbo-machinery blade is a challenging and iterative process where a number of targets have to be met. Table 5.1 shows a list of major design constraints and variables that need to be checked during the design phase. Therefore it is highly recommended that the blade design should be parameterized. Parameterization not only eases the design process but also minimizes time and cost. This section deals with the parametric blade profile design, blade profile optimization, stacking, 3-Dimensional CAD modeling and grid generation process.

Table 4-1 Checklist for Blade Design

CONSTRAINTS AND DESIGN TARGETS IN BLADE DESIGN	
MECH CONSTRAINTS	TIP SPEED, OVERALL DIAMETER AND AXIAL LENGTH OF THE STAGE
MANUFACTURING CONSTRAINTS	BLADE STACKING, RADIAL SMOOTHING, 3 D BLADING, END BENDS, CASING AND HUB TREATMENT
THERMODYNAMIC CONSTRAINTS	ENTHALPY DROP AND MASS FLOW RATE
AERODYNAMIC CONSTRAINTS	INLET EXIT ANGLES, MACH NUMBER, TURBULENCE RATIO, PASSAGE AREA, THROAT AREA, STAGGER, CAMBER, POSITION OF MAX THICKNESS, CURVATURE DISTRIBUTION ON BLADE, TIP LEAKAGE FLOW, END WALL TREATMENT, LE AND TE GEOMETRY, BLADE ANGLES, FLOW ANGLES, WEDGE ANGLES AND BLADE TAPER
THERMAL AND AEGING	CREEP AND THERMAL FATIGUE
VIBRATION CONSTRAINTS	TORSION AND BENDING MODES AND NUMBER OF BLADES
OTHER CONSTRAINTS	AERO-ELASTICITY, LIFE

4.1 Creation of Blade Geometry

The process of generating the blade geometry can be divided into two parts. The first part is choosing a basic blade shape, e.g. a conventional blade profile, and imposing design parameters and carrying out CFD analyses in order to achieve the design targets evolved from the preliminary design calculations. The second part is to optimize the blade profile by state of art approach and derive maximum performance out of it. One of the best method of optimization is through Artificial Intelligence, e.g. ANN.

The outcome of preliminary and detailed design desired the nozzle to features 11 vanes with aspect ratio of 0.65, a turning angle of 62°, and exit Mach number, subsonic at the vane mean section, corresponding to an isentropic nozzle pressure ratio of 1.55. Details of the nozzle design and midspan geometric parameters are presented in Figure 4.1. The dotted lines show tip and hub sections. The rotor features with 14 blades. It is designed for sub impulse conditions at the blade root, with a resultant large flow turning of 65.23° and a high inlet relative Mach number.

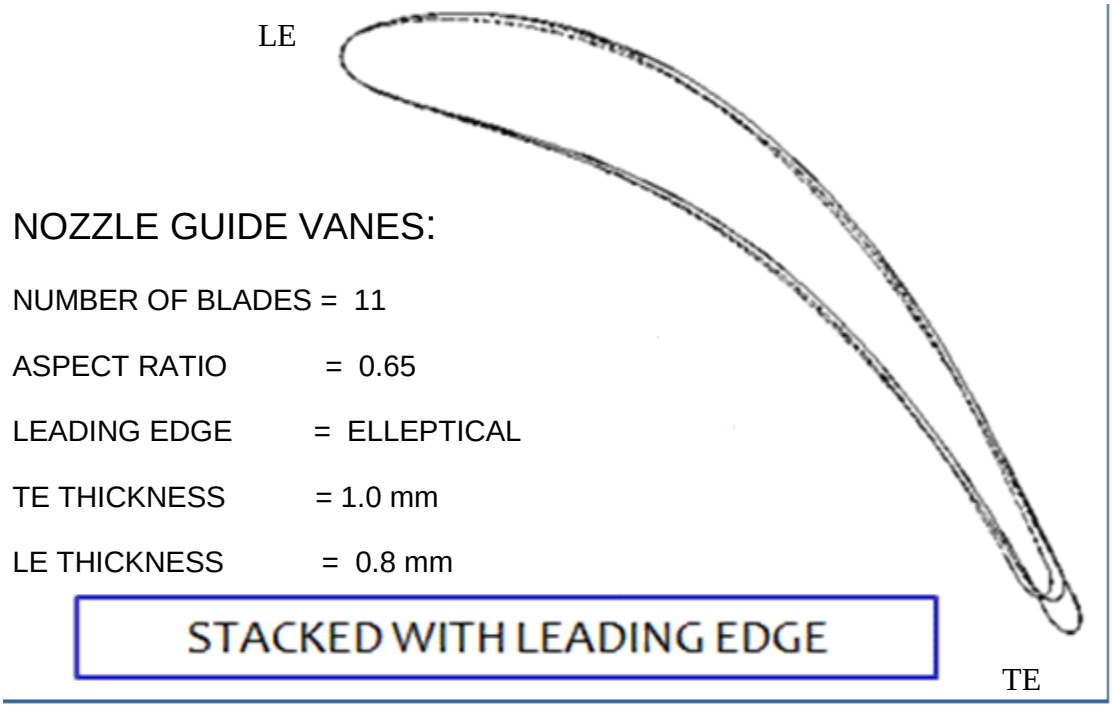

Figure 4.1 Stacking of Stator Vane

Using these data, blade profiles were generated in Numeca Environment. The thickness distribution is one of the important criteria in blade design. The position of maximum thickness was chosen to be 0.36% of blade chord for both rotor and stator. The dimensions of the leading and trailing edges were chosen 1mm and 0.8 mm respectively, allowing for the feasibility in manufacturing and also considering aerodynamic stability and blade vibrations. On the other hand, smoothness of the profile was given more significance to avoid any local pocket of shocks on the profiles during its operation. A stagger angle of 35° was imposed on the rotor and 40° on

the stator after iterative studies.

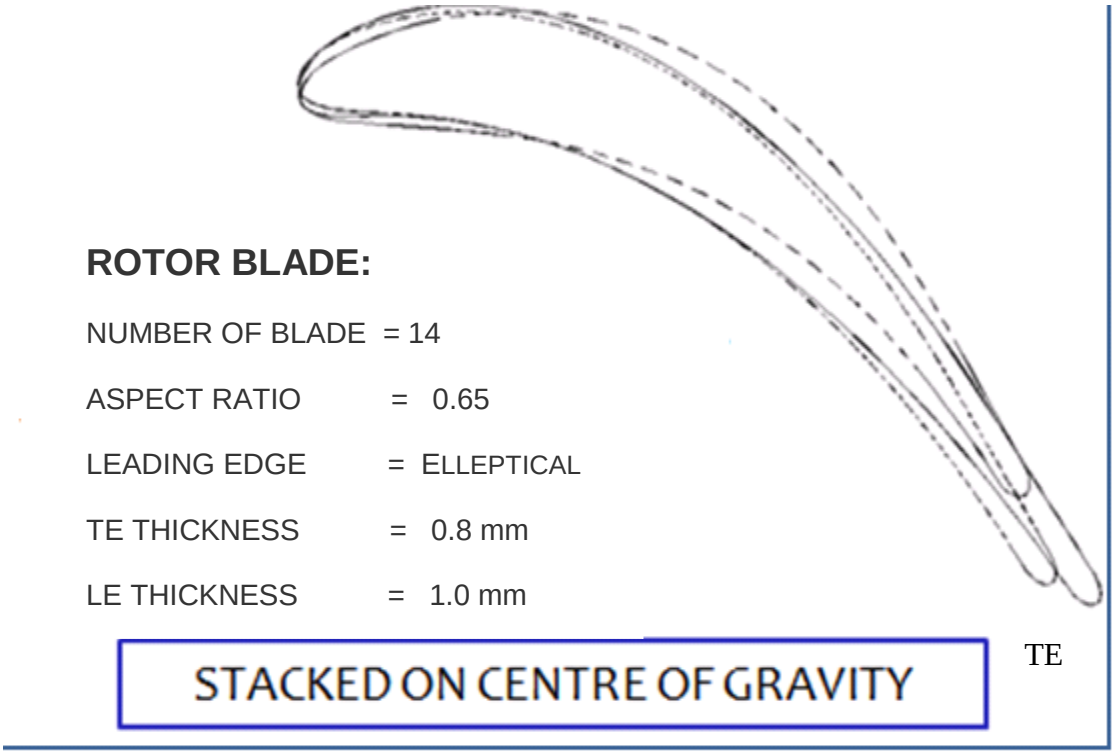

Figure 4.2 Stacking of Rotor Blades

Blade count was also an important parameter that influenced blade loading. It was found that higher number of blades reduced the magnitude of loading on each blade, whereas increased the blockage in the flow path and vice versa.

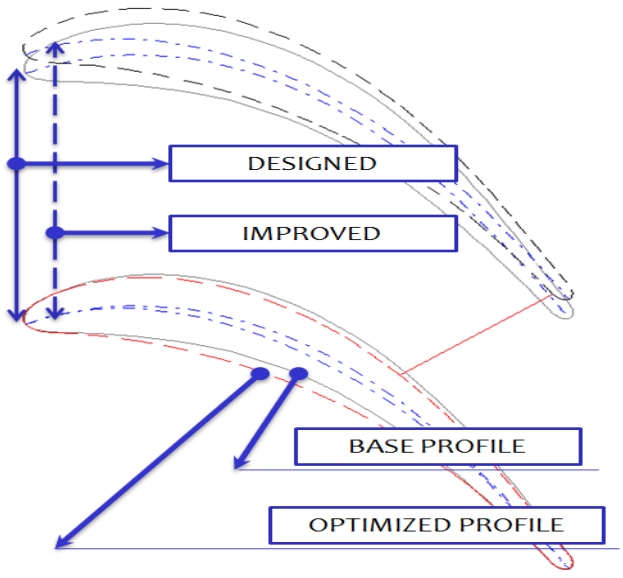

Figure 4.3 Optimal and Base Blade Profile

A number of such iterations yielded an optimal number of blades to be 11 and 14 on stator and rotor respectively.

A profound understanding of the flow conditions enables the designer to optimise the aerofoil profiles for a given flow condition. But since the methodology

adopted here was manual, it needed a lot of such iterations to arrive at the optimal profile. Also, it required CFD runs to assess the performance at each step. A couple of profiles that showed improved performance than the former base profile are shown in Figure 4.3. Dotted lines in the figure indicate the base profile.

Since, this method of blade generation was manual and necessitated CFD runs at each step to assess the performance and get an idea of improvement in the corresponding step, the time investment became a major factor of concern. So there was an urge for a better method, which would give optimised profile parameters that saved time. Pierret and Braembussche [11] have mentioned the implementation of Artificial Intelligence in the blade generation process. Therefore, a method of Artificial Neural Network (ANN) was implemented for the future runs. The use of ANN gave a genuine idea of performance without running CFD computations.

A two layered multi-input and multi-output ANN was therefore developed and the same is shown in Figure 4.4. The inputs usually involve a set of blade geometric and aerodynamic parameters like lengths of control points, stagger angle, throat area, mass flow rate, etc. The network was trained to arrive at the weights. The summation was a sigmoid function of values varying between 0 and 1. Finally an idea of inputs required to achieve the desired output was obtained.

4.1.1 3D Modelling of Nozzle and Rotor Blisk

Upon finalising the 2 D blade profiles, a 3-D geometry was generated for stator and rotor vanes. Disc portion of the rotor blisk was further modelled in ANSYS design modeler as shown in the Figure 4.5. The summary of steps that were involved in the modelling of rotor blisk is given below:

Step 1: The vane sections were stacked such that the LE was straight and radial in the meridional and axial views using NUMECA software as shown in Figure 4.1

Step 2: Rotor blades was stacked with respect to centre of gravity of each airfoil sections as shown in Figure 4.2. A single blade surface was formed during this process.

Step 3: The blade surface formed was and imported into ANSYS design modeller in Inter Graphics Exchange Specification (IGES) format.

Step 4: The disc portion of the rotor was obtained by revolution of the disc section.

Step 5: Pattern feature was used to repeat the number of blades around the axis.

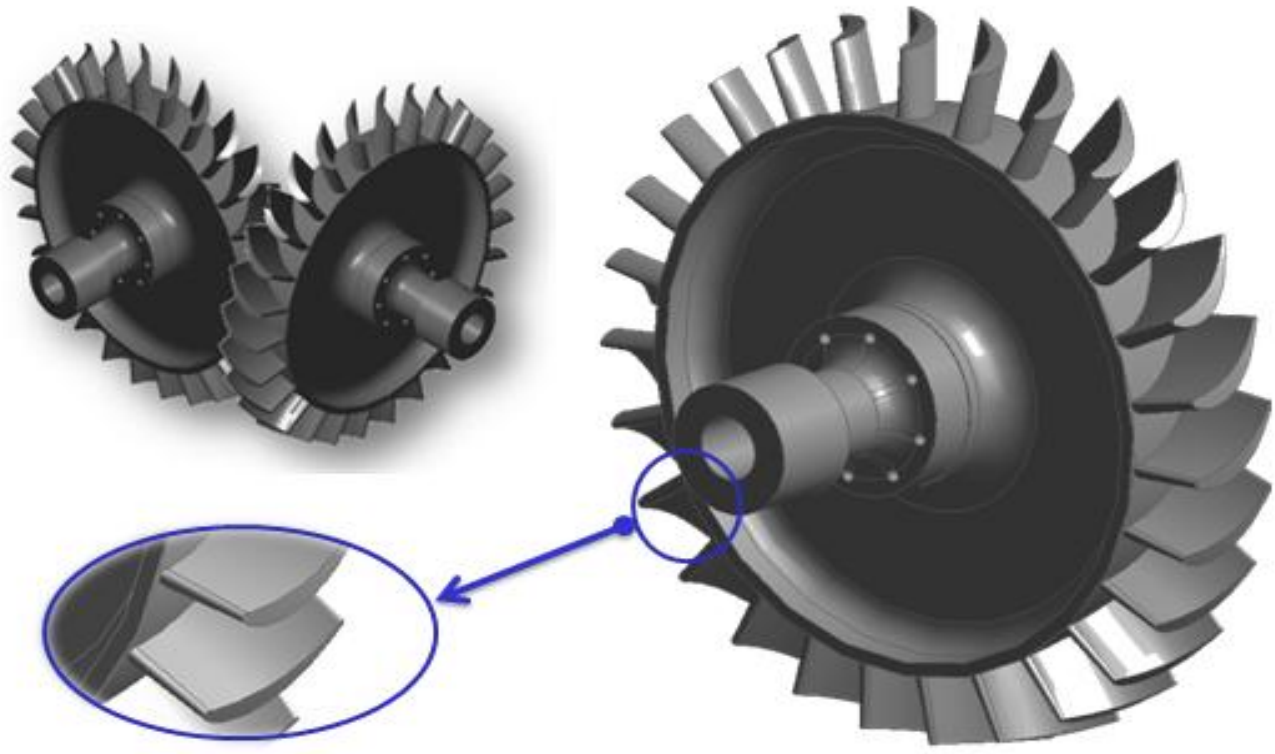

Figure 4.4 3D Geometry of Rotor Blisk

An outlook of manufacturability was also thought of in the process. Figure 4.4 shows a three dimensional model of turbine rotor blisk with coupling and shaft arrangement

4.2 Aerodynamic Analyses

4.2.1 Grid Generation for CFD Analyses

Grid generation is one of the most important steps for numerical modelling. The solution depends to a large extent on the grid. Therefore, the grid should be such that it should be able to resolve the complex flow features of modern gas turbine components. The grid should be clustered towards the wall for resolution of the boundary layers. Further, there should be around 10 to 15 points inside the boundary layer. The grid should also be orthogonal with respect to the

wall for proper implementation of the wall boundary condition. Smoothness within and across the various blocks is also desirable. The grid density should be high around the leading and trailing edges for proper representation of the blade geometry. The expansion ratio and aspect ratio are some of the other properties which are used to evaluate the grid quality. Lastly, the grid should not contain any negative volumes.

The grid generation in Numeca Autogrid is automated for turbomachinery blades and minimum inputs are required from the user. Grid was generated individually for the NGV and the rotor and the two grids were merged in IGG as shown in Figure 4.6

4.2.2 Grid on Nozzle Guide Vanes

The first stage nozzle guide vanes of a gas generator turbine are subjected to strong loads, not only because of the aerodynamic impacts on the blade geometries owing to their smaller dimensions but also because of high temperatures involved.

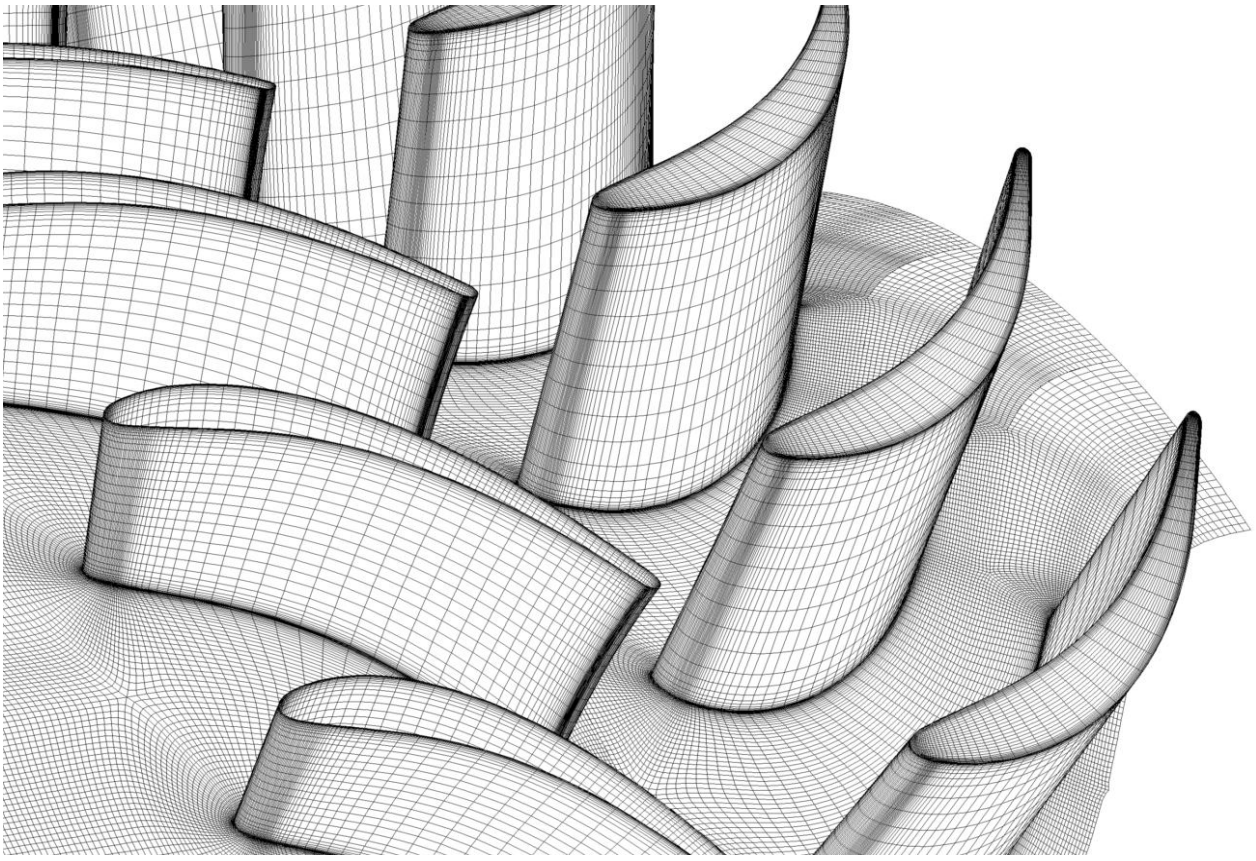

Figure4.5 Multi-Block Computational Mesh of Rotor and Stator

Multi-block grid is chosen to ensure adaptively in such fields. However, there is a freedom of selecting number of nodes on the profile as the flow is subsonic and there is no problem of shocks in the trailing edge region. For accuracy, many nodes were taken in the stream wise direction to capture the flow physics at the trailing edge. The only problem in having many nodes is that it leads to much heavier computing time. However, a compromise should be made to select the economical solution

4.2.3 Meshing of Blade Channels

The computational domain was divided into sub-domains like blade and tip clearance region and each of which supported a structured grid as shown in the Figure 4.6 The approach chosen to generate the grid for a rotor with tip clearance was similar to the one generated for stators. A radially stacked mesh, formed by 2-D multi-block grid surfaces, extended from hub to shroud, thus leaving a gap in the tip clearance region. The grid lines were clustered towards hub and the casing to capture the end wall boundary layers correctly.

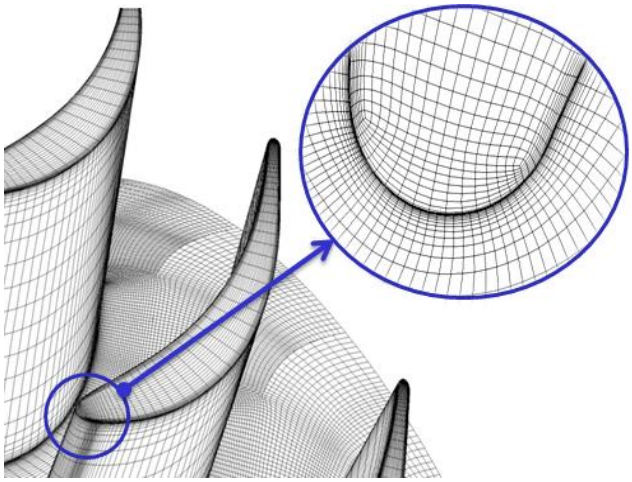

Figure 4.6 Typical Tip Clearance Meshes

4.2.4 Meshing of the Tip Clearance

The gap left in the O mesh between the blade tip and the shroud was divided into two sub-domains formed by an O mesh and an inner H mesh. Both the sub-domains extended radially equidistant and got stacked from the blade tip to the casing.

Only the surface corresponding to the blade tip and the one corresponding to the shroud coincided with the outer grid surfaces with their coinciding grid nodes. The total number of grid points was equal to 731958 and comprised of 6 blocks,

4.3 Boundary Conditions for CFD Analyses

In Order to describe the flow physics accurately and to obtain a good quality of the numerical results, special care must be paid to the treatment of the boundary conditions.

The following are the boundary conditions imposed on the axial turbine stage:

1. Total pressure, total temperature and flow direction at the inlet
2. Radial equilibrium back pressure at the outlet
3. No slip boundary condition on the walls
4. Periodic boundary condition at the blade to blade passage
5. Mixing plane approach at the rotor-stator interface

The stage inlet flow angles were set to 20°. The total temperature and total pressure profiles were 999.42 K and 249013 Pa respectively. A radial equilibrium back pressure of 102346.8 Pa was imposed at the exit. Air was considered as the real gas and the values of C_p and specific heat ratio were taken as 1140.40 J/kg/K and 1.3362 respectively at the temperature of 999.42 K.

4.4 Computational Details

The one equation Spalart-Allmaras turbulence model was used in all the computations and the equations were solved by central difference scheme. Multigrid and implicit residual smoothening were used for convergence acceleration. The hub wall of the rotor was given rotation along with the blade while the NGV hub and entire shroud were stationery. Implicit Residual Smoothening and Multi-Grid Acceleration were used for convergence acceleration of the solution.

4.5 Mechanical Analyses

The airworthiness requirement of any component in an engine design process necessitates that the component be durable and safe even under off-design conditions. Hence, it is challenging for a designer to meet these requirements while increasing the shaft power to weight ratio. The structural design phase therefore plays a huge role in the design of an engine.

For instance, the failure of turbine blades may destroy the containment and static structures, thereby leading to failure of the whole aircraft by impact. Similarly, the burst of the

disc may lead to catastrophic failure. Therefore, in the current study, emphasis was given on disc design to find its minimum thickness even under 115% overspeed. And as a goal of weight saving, the disc was optimized for its weight, still keeping the stress levels and frequency of excitations well within the limits

4.5.1 Meshing of Disc

Meshing is a technique in which the solid model is discritised into number of finite elements in order to capture the physics of the model under given loading and boundary conditions. As grid generation is carried out before the CFD analysis, computational mesh is generated before FE analysis also. The method of mesh generation, the element quality and the type of mesh defines the accuracy of the solution.

The process of meshing was done in ANSYS Workbench 11.0. Mesh generation in Ansys is simple and involves auto generation. The model was meshed with all tetrahedron elements.

4.5.2 Boundary Conditions and Loading

Since the design of turbine blisk is very complex, involving a number of loads, the classification of loads becomes a challenging task. For instance, in the present case, as the rotor is rotating at very high speed of 43000 rpm, the disc web, rims and the blades are subjected to high centrifugal load. As a result, high hoop stresses and radial stresses are developed. Hoop loads are very harmful as they may lead to bursting of the disc at higher speeds. Apart from the centrifugal load, the other major loads are gas loads.

In order to simulate the realistic state, a cylindrical joint boundary condition was imposed on the blisk and the working environment was set to 950° C. And as far as the loads are concerned, the gas loads on the blade were imposed.

5 – Validation and Discussion of Results

The present section contains the results obtained for a high performance single stage axial turbine. It centers mainly on CFD and mechanical analyses. In the first section the validation of computational codes, NUMECA and ANSYS, have been dealt to evaluate their suitability for application to the stage design of the axial turbine. The second section deliberates on preliminary design, detail design, CFD computations at design point and comparison of the CFD results with design targets. These design targets however were set from thermodynamic analysis of the gas turbine cycle. The influence of parameters like rotor tip clearance and nozzle stagger angle on the performance of the turbine are also discussed in detail. Furthermore, a structural analysis on the rotor blisk is performed in order to determine the minimum web thickness of the blisk, morphing for uniform strength and optimise for its weight based on design of experiments.

5.1 Validation Studies

The validation of the codes was performed in two steps: one by analyzing the Aachen turbine [18] of 1.5 stages and comparing NUMECA results with the experimental values and other popular turbo-machinery codes. The second was by mechanical studies on a simple disc and comparing the ANSYS results with analytical values.

The Aachen turbine is an axial flow turbine consisting of three blade rows: the first vane, the rotor blade and the second vane. The second vane is exactly the same as the first vane. The blade counts for stator and rotor are 36 and 41 respectively. The inlet total pressure and outlet total pressures are 166871 Pa and 112500 Pa respectively, with a rotor speed of 3500 rpm. The grid was generated taking 4 blocks with 890124 points and radial equilibrium BC's were imposed at the outlet. Jameson-Schmidt-Turkel scheme [19] and the one equation Spalart Allmaras turbulence model [20] was used for computations.

Comparison studies were made between NUMECA and the results obtained from 'TFLO', United Technologies' solver '3D FLOW', NASA/GE's solver 'APNASA-V5' and the experimental data. The circumferentially averaged total pressure, total temperature and absolute flow angle at the rotor exit, 8 mm after trailing edge, of vane and rotor were considered for comparison. The validation of ANSYS for structural analyses was done by analysing a simple disc rotating at 43000 rpm. Due to very high disc speed, it was subjected to combined hoop and

radial stresses, which might have lead to bursting of the disc at web sections. The computations were evaluated at this speed and the results were compared. It is found that the results are in agreement with analytical values, as shown in the Figure 5.2.

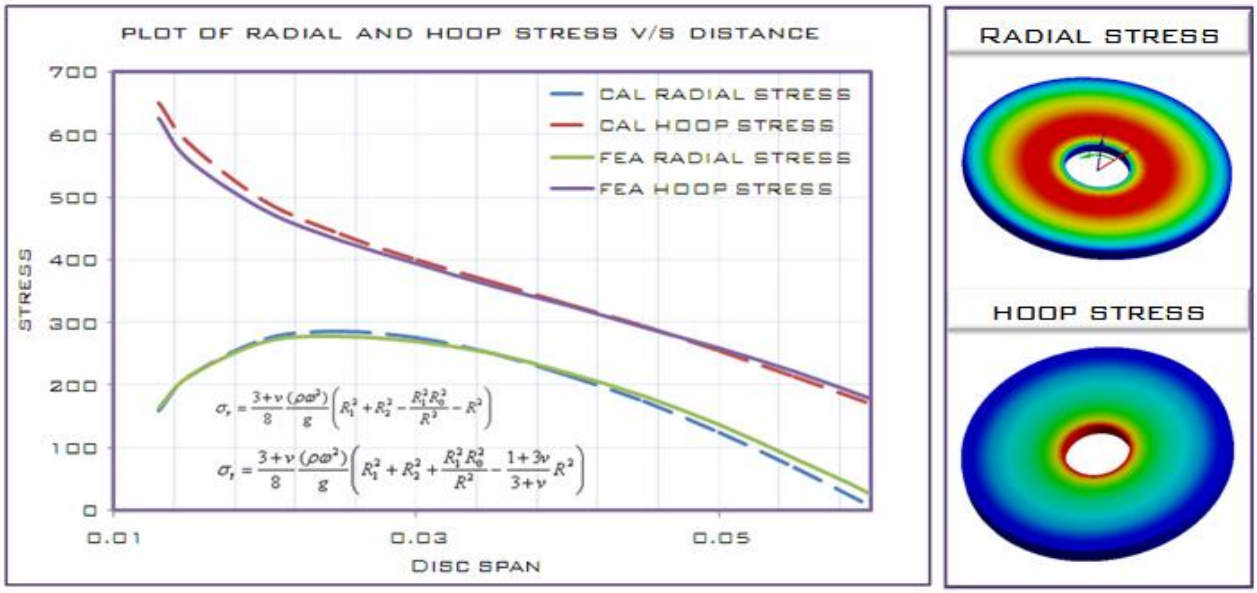

Figure 5.1 Code Validation Study; Simple Disc Analysis

The dotted lines in the Figure 5.2 indicates the analytical values for hoop and radial stress where as the continuous lines indicates the same from computations. It can be observed that maximum value of the hoop stress occurs at the inner radius and the maximum value of radial stress occurs at a distance as given by equation 5.1

$$R = \sqrt{R_i R_o} \qquad \ldots\ldots (5.1)$$

5.2 CFD Analyses at Design Point

CFD analyses were carried out on the turbine stage for the optimum point 'P' on the design space as shown in Figure 3.1. At the design point, a mass flow of 1.96 kg/s at an adiabatic efficiency of 90% was obtained for an expansion ratio of 2.0579. The turbine stage generated a torque of 70.88 N-m and power output of 315 kW. The results obtained by analysing the design point are discussed in the following sections:

5.2.1 Static Pressure Plot

Figure 5.5 shows the static pressure distribution for both the nozzle and the rotor at hub, mean and tip sections. The smooth drop of static pressure can be seen from the figure, especially at the mean section. At the hub and the tip, a modest flow deceleration is observed on the suction side. A number of CFD runs were executed to improve the flow conditions and hence the performance of turbine. It was observed that a minor change in blade profile can even lead to a significant change in efficiency and mass flows.

Several iterations were performed sequentially for various blade profiles. Each such iteration involved profile generation, stacking and performing CFD analysis. Improvements for the next level of iterations were gathered from the experiences gained by pervious steps. Finally a profile was selected, that had an efficiency of 90.01% and a mass flow rate of 1.964 kg/s. A further modification in profile led to the blockage at throat area of the stator. Figure 5.3 shows the preliminary profile of the blade which formed the base profile to generate an improved one. Improvements were extracted in terms of reduction in Mach number and efficiency. The improved profile was considered as the optimized profile and Artificial Neural Network was developed based on the geometric parameters associated with this profile.

5.2.2 Mach Number Plot

Figure 6.5 shows the Mach number plot at hub, mid and tip sections. Smooth acceleration of flow can be observed towards rotor and stator exit passage. Though the pockets of local acceleration are observed on the suction side of the profile, they do not lead to any shocks. The azimuthally averaged Mach number plot (Figure 5.4) at the nozzle-rotor interfaces gives an inference of the increase in the Mach number towards hub. Again, since the flow is subsonic at the nozzle hub, the passage does not get choked and confirms to the design.

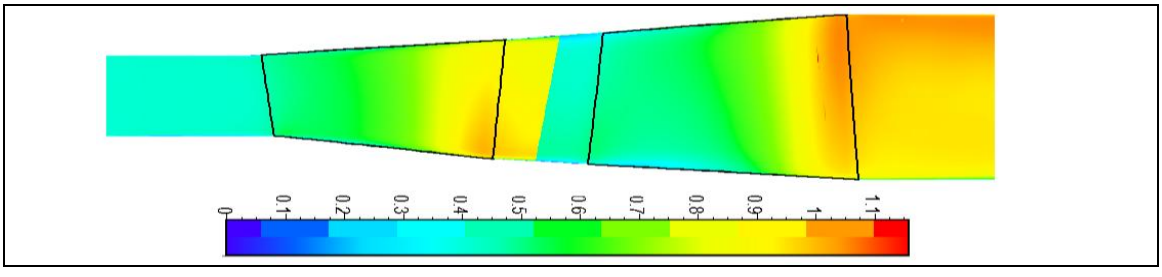

Figure 5.2 Meridional View of Mach Distribution

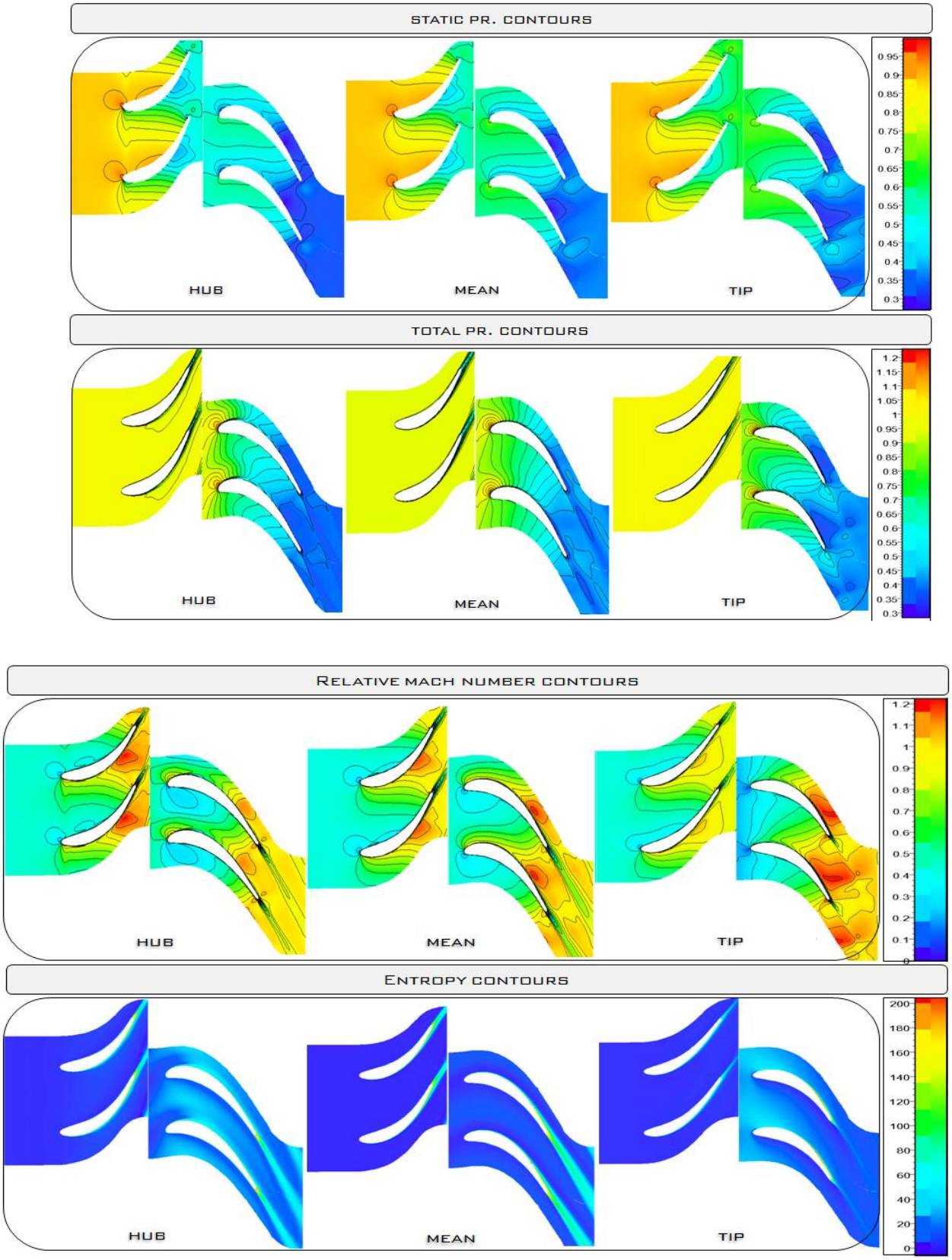

Figure 5.3 (a) Static Pressure Contours (b) Total Pressure Contours (c) Relative Mach Number Contours and (d) Entropy Contours

5.2.3 Total Pressure Plots

The total pressure plot at hub, mean and tip sections of the rotor and stator are shown in the Figure 5.5. As expected, the drop in total pressure can be seen mainly in the rotor section where as the losses due to boundary layer occur both in the nozzle guide vanes and the rotor blade passages. The total pressure recovery for the nozzle is around 96 to 97 %. A further improvement in pressure recovery of up to 98-99% can be obtained in the nozzle through extensive CFD experiments. Figure 5.6 shows the total pressure at rotor stator interface. The total pressure remains almost constant at the interface.

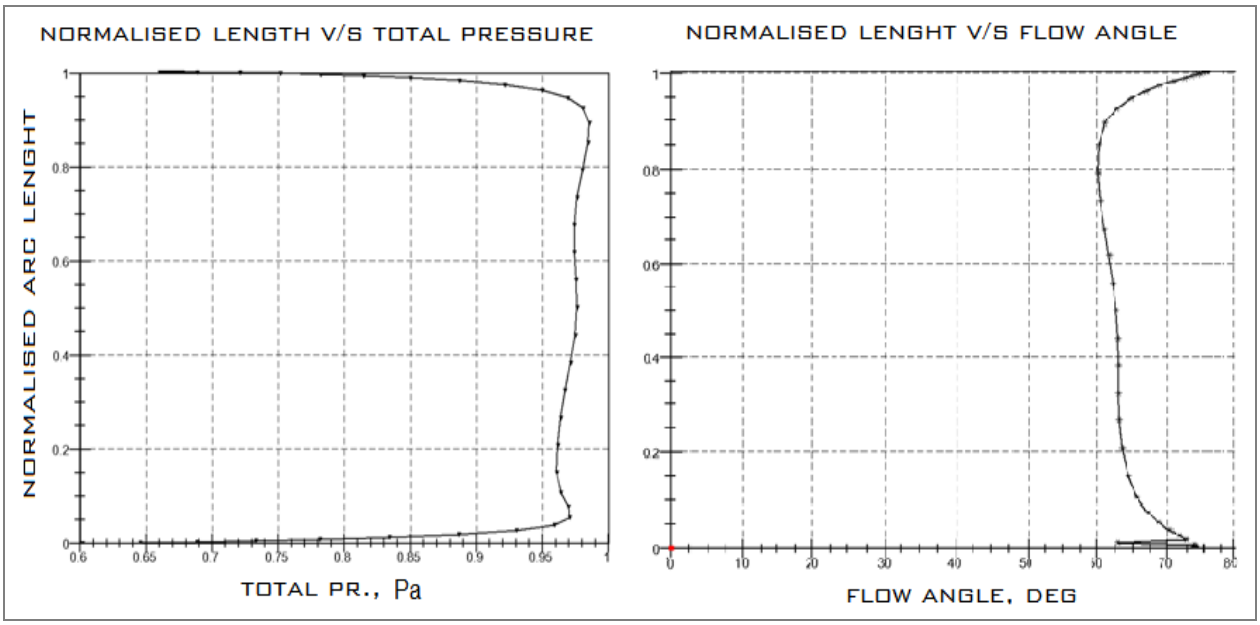

Figure 5.5 Azimuthally Averaged (a) Total Pressure Distribution and (b) Flow Angle Distribution at Rotor-Stator Interface

5.2.4 Entropy Plots

Entropy plot at the hub, mean and the tip sections are shown in Figure 5.5. Production of entropy in the free stream flow is negligible whereas there is considerable entropy production at the hub and the tip sections. While the entropy production at the hub can be attributed to the random flow near casing, the entropy in the tip is mainly due to tip clearance vortex. The reduction in disorderliness at the hub can be achieved through improvements in the blade profile, casing profile and their interface whereas the reduction in entropy production in the tip can be achieved through extensive tip clearance studies.

5.2.5 Flow Angles

The azimuthally averaged flow angle distribution in the nozzle-rotor interface is shown in Figure 5.5 The flow angles are very close to the designed values from the preliminary design calculations. A comparison of flow vectors at hub, mid and tip is also shown in Figure 5.7.

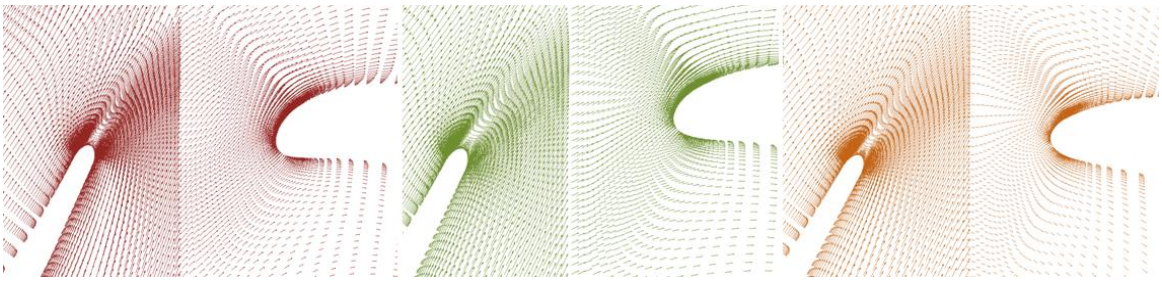

Figure 5.6 Vector Plot of Flow Angle Distribution at Hub, Mean and Tip Sections

5.2.6 Velocity Vector Plots

The velocity vectors at rotor-stator interface are shown in Figure 5.7. It is seen from the figure that the flow is aligned to the blade and deviation in the nozzle trailing edge is negligible. Further the incidence to the rotor is very good with the flow angles being closer to the rotor blade angles. The velocity vectors in the tip region were showing the flow cross over from the pressure side to the suction side. The velocity stream line a plot showing the cross over phenomena at the tip region is shown in Figure 5.7 .

5.3 Design parametric Studies

The purpose of parametric studies is to evaluate the performance of the turbine at off design conditions. The off design conditions may exist in the turbine operation because of adverse conditions like change in altitude and attitude of the flight. For example, the turbine operation may also vary due to the influence of relative radial expansions of the rotor and casing due to changing engine temperature levels.

In this section, the effects of stagger angle and tip clearance are the two parameters that are studied. The first test case is the study of stagger angle, especially that of nozzle. The stagger angle is varied between 35°, 40° and 45°. A very interesting test case is that of tip clearance. The tip clearance gap is varied over three different values: 0.5%, 1% and 1.5% of the blade span and their effect were evaluated with respect to the performance characteristics of the turbine stage.

5.3.1 Effect of Vane Stagger Angle on Performance Characteristics of Turbine stage

The stagger angle is the angle between the airfoil axial chord and the airfoil chord. As discussed, the nozzle stagger angle has a vital impact on the performance of the turbine stage as it influences the inlet Mach number to the blade and certainly the incidence. Many investigations have been already carried out in the past and found that higher stagger of nozzle yields better performance. This section deals with the studies that were carried out by 're-stagger' of the nozzle vanes. The difficulty faced while re-staggering process was the throat area being reduced and leading to choke the flow passage. The study here is to evaluate the performance for higher stagger angles without altering the throat area.

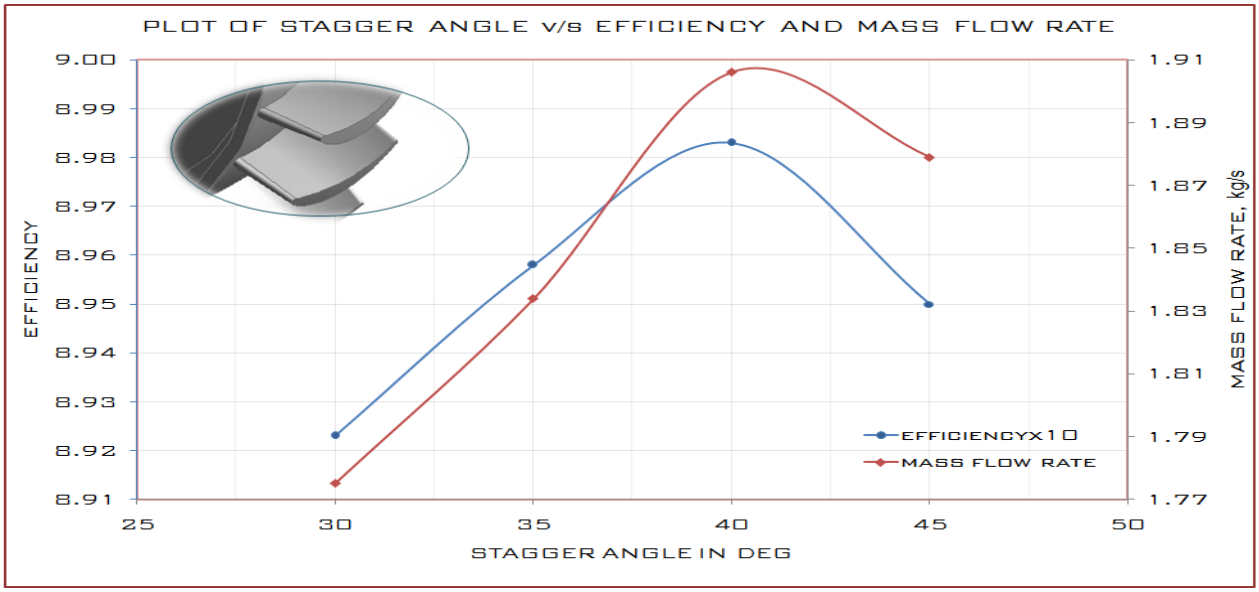

Figure 5.7 Parametric Study of Vane Stagger Angle

Staggering was provided to the blade profile by inputting stagger values and in NUMECA software. Though these profiles were modified with an intention of maintaining a constant throat area, a strictly fixed throat area was difficult to achieve for all these three cases. This is because the extreme of profile modification would lead to distortion of blade profile. A compromise was made to accept the minimum throat areas for higher stagger angles. Finally the CFD studies were executed with stagger angle of 35°, 40° and 45° at a constant N /√T value of 1530.

Figure 5.8 shows the variation in efficiency for change in stagger angle at a constant blade speed. As expected, the performance improved in terms of efficiency as the stagger was increased from 35° to 40°. But interesting results were found when stagger was further increased to 45°. It was found that efficiency was tending to decrease with the increase in stagger beyond 40°. This can be attributed to the fact that even a small change in throat area can lead to mass flow variations across the turbine stage.

5.3.2 Effect of Tip Clearance on Performance Characteristics of Turbine Stage

Tip clearance effects are considered to be one of the major sources of efficiency loss in un-shrouded turbines and are believed to be the principal mechanism for dissipation of kinetic energy through the gap. Tip clearance losses account for about 45% and 30% of the total losses in the rotor and the stage respectively of a high pressure turbine. Therefore one would expect that the strength of the clearance vortex would increase with increase in tip clearance distance. Tip clearance not only alters the blade loading but also affects the flow turning ability of the blade thus affecting the performance of the turbine.

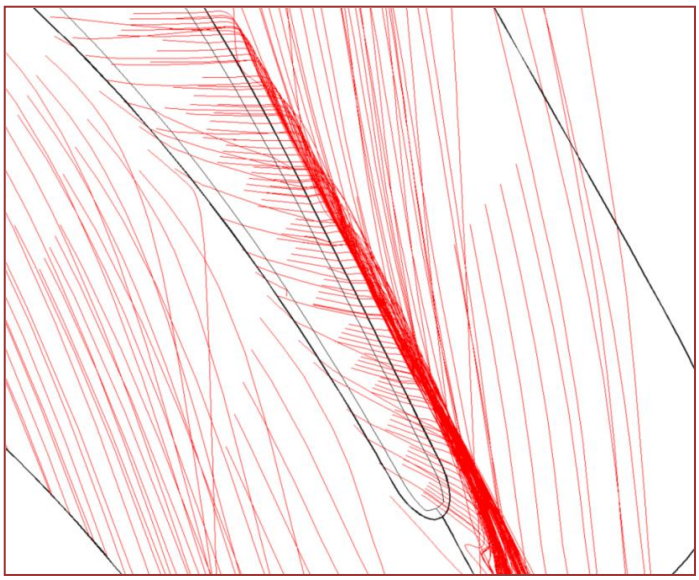

Figure 5.6 Cross Flow at Tip Region

In order to assess the performance of the turbine stage for varied tip clearances, the parametric studies were conducted with a tip clearance of 0.1 mm, 0.15 mm, 0.2 mm and 0.25 mm respectively. Figure 5.9 shows the variation of turbine stage efficiency for varied blade tip clearance at the designed speed of $N/\sqrt{T} = 1530$. It was found that the efficiency variation is non linear with an overall efficiency reduction of 1.93 % for a difference in gap of only a 0.15 mm. It can also be observed that the mass flow rate increases as the blockage reduces with the increase in clearance.

Tip clearance generates a strong tip leakage vortex, and while the tip clearance vortex appears to improve the overturning effect of the secondary flow vortex, it actually damages the performance of rotor blades because it causes the blade tips to unload. The effect of the tip leakage flow is shown in Figure 5.9. As expected, it was noticed that when the tip clearance is increased, the vortex becomes bigger and stronger and blade reaction reduces. This reduction in reaction led to performance deterioration.

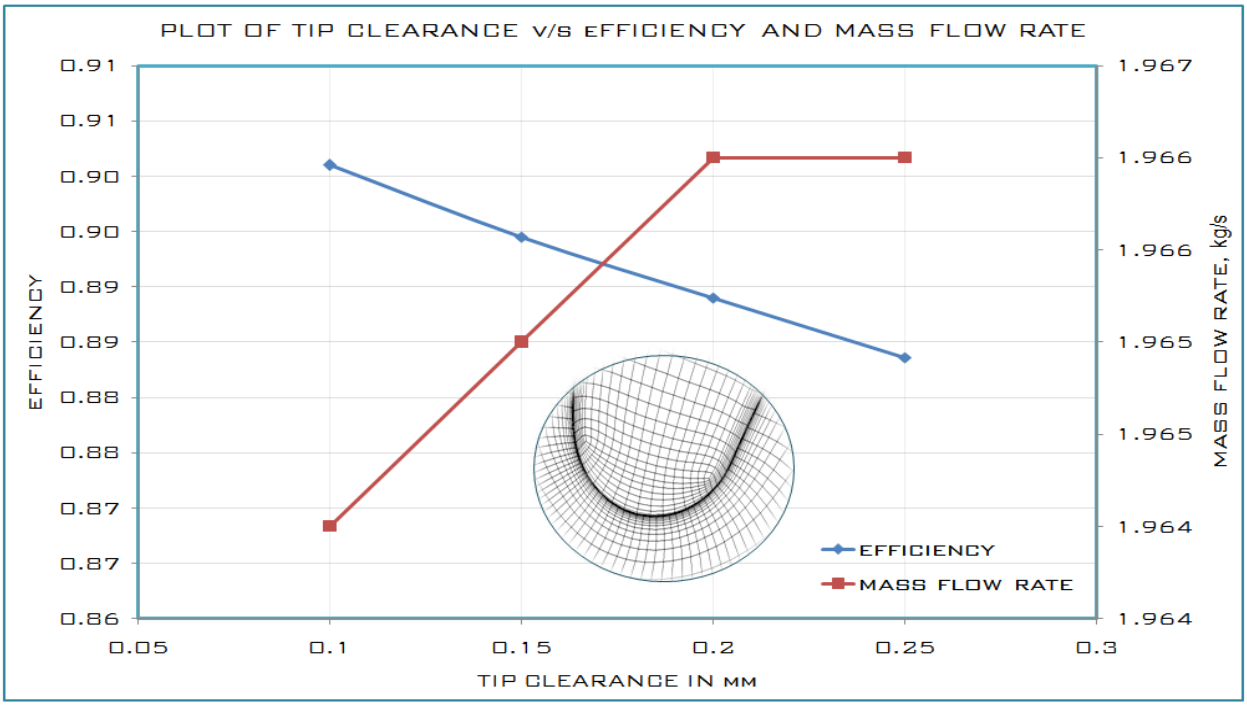

Figure 5.7 Parametric Study on Tip Clearance

5.3.3 Conclusion of Parametric Studies

The change in the vane stagger contributes only to a certain extent to the efficiency variation. The dominating effect is the flow across the blade tip and the vortices associated with it. This is because the losses due to the tip flow are not restricted to the immediate vicinity of the blade tip area but spread radially inwards with increasing tip clearance covering nearly 25% of the blade span at relative clearance values of 0.5% to 1.9% of the blade height. This becomes evident from Figures 6.8 and 6.10 which show the variation of efficiency and hence performance distribution. These results show the necessity of careful casing and rotor design in the design of an axial turbine stage.

5.4 Performance Plots

In the design of the turbine stage, since the goal is to obtain a high performance design configuration, a design point 'P' will be derived and fixed based on several iterative studies as discussed in Section 3.1. It becomes obvious that the final design parameters based on this point 'P' yield a best performance. The thermo-physical properties associated with this point are therefore significant and need to be maintained during the turbine operation. Perhaps it is undesirable that the same design point could be sustained. There are many possibilities for this and few of the causes would be change in altitude of operation, off load and over load. It may also happen due to losses associated within the system. Hence it is necessary that off design conditions are evaluated, thereby confirming the flexibility of the turbine operation.

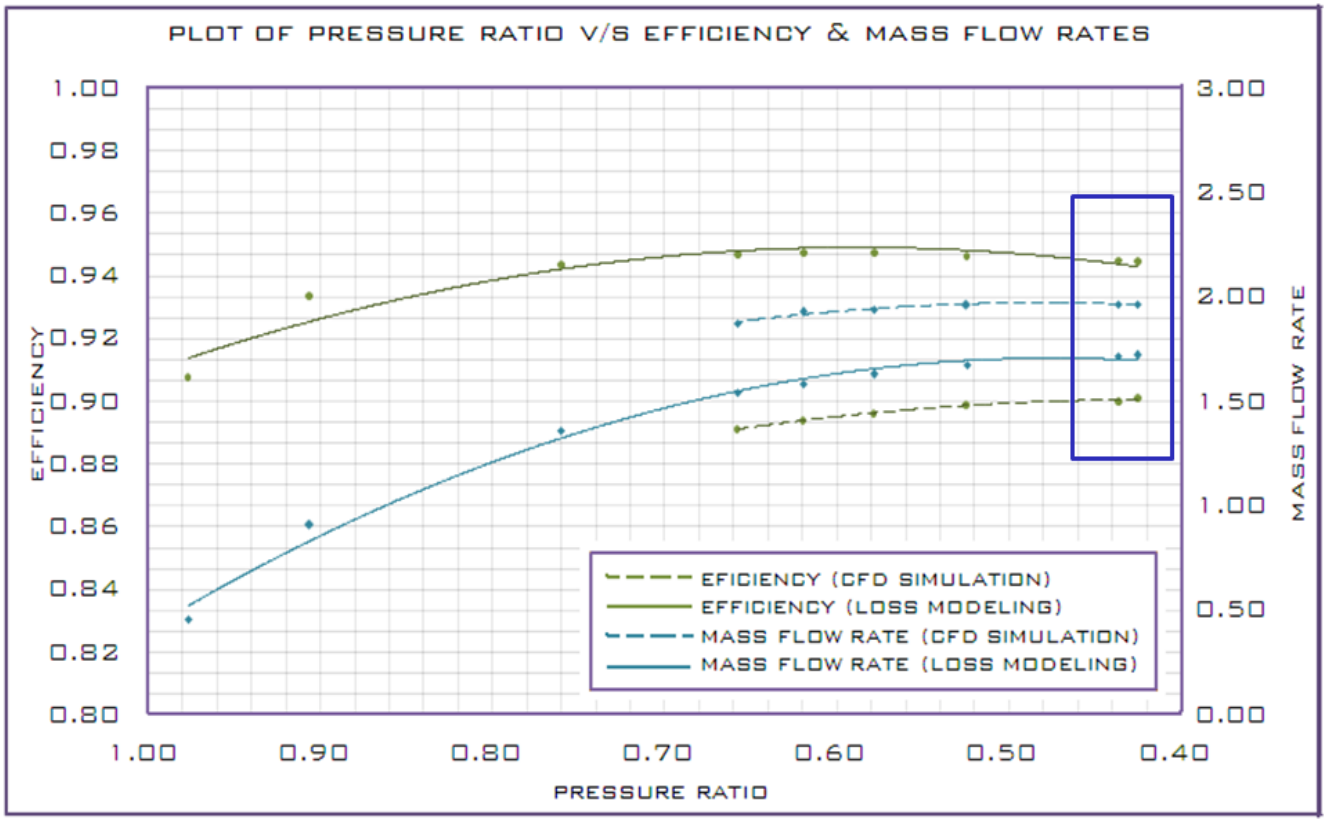

Figure 5.8 Performance Plot of Axial Turbine Stage

The influence of off design condition on turbine stage efficiency can be seen from Figure 5.11, where the relative isentropic efficiency is plotted as a function of stage total pressure ratio.

The process of performance plot generation involved varying the back pressures arbitrarily for a fixed turbine speed of 43000 rpm and executing CFD analyses on each off-design case. From Figure 5.11, it can be noticed that for lower mass flow rates, the flow is subsonic and the efficiency levels are also lower. The exit Mach number levels of a turbine operation therefore depend on the stage pressure ratio and the size of the throat area. At high stage pressure ratios, more than 2.34, both the cascades are choked and again the efficiency drops. The choking process and its influence on the efficiency of the turbine stage can be realized when mass flow rate becomes constant for further change in back pressure as shown in Figure 5.11 by a highlighted block.

This study shows the importance of a careful control of the airfoil loss characteristic as well as the vane and blade area matching.

5.5 Mechanical Analyses

Since the turbine is a very complex system rotating at very high speeds of 43000 rpm, it experiences a number of major loads like centrifugal load, gas load and thermal

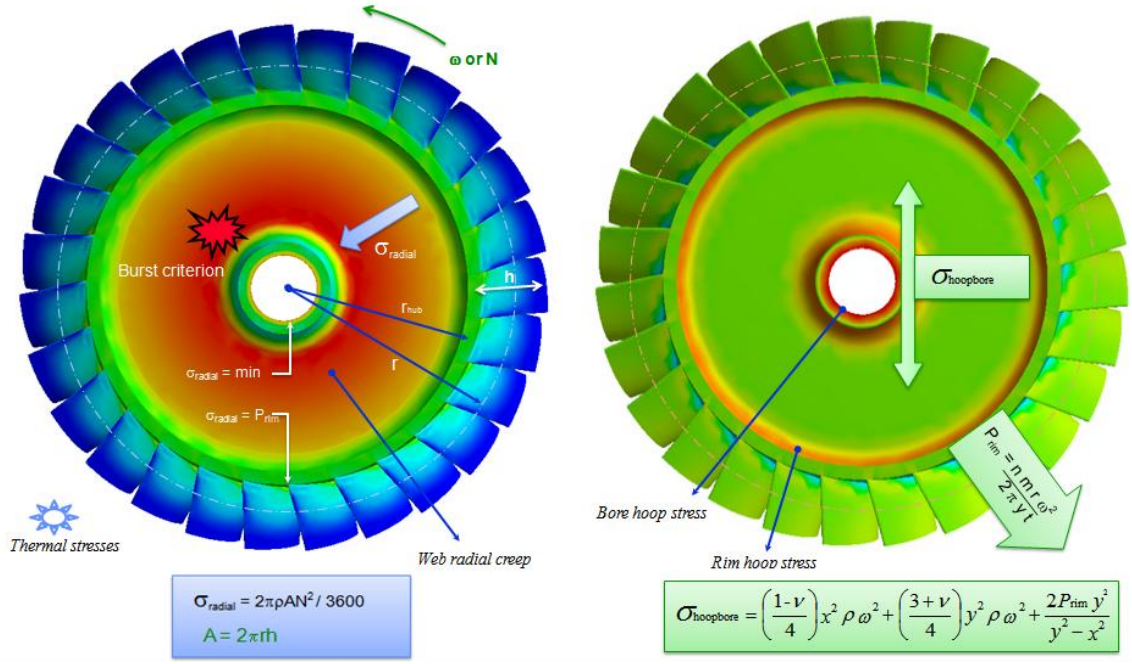

Figure 5.11 Radial and Hoop Stress Distribution on Turbine Blisk

The influence of the radial stress in the rotors is to burst the web of the disc at higher speeds where as the hoop stresses lead to crack initiation and propagation at the hub. Hence both of these loads are harmfull for the turbine operation and needs care to be taken in the mechanical design stage of the turbine design.

5.5.1 Parametric Study: Minimum Thickness of Blisk

As discussed in the previous section, design of a rotor disc is one of the important tasks in mechanical design of a turbine and needs several criteria to be met for its safe operation. The various design criteria include considerations on creep life, burst margin and low cycle fatigue in addition to blade dynamics and related HCF.

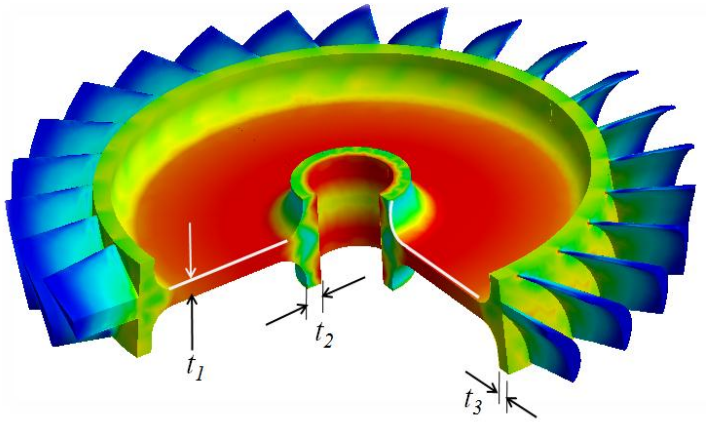

Figure 5.12Mechanical Design Parameters

From manufacturing point of view also, relative ease is expected in producing it. All these factors ensure that it is just not possible to increase or decrease the thickness of discs as desired. It is therefore required to find a minimum thickness of bladed disc that overcomes mechanical limitations as well saving weight of the component. Weights of the components in airborne engines have a high significance because saving the weight on each individual component can save overall weight of the aircraft, and hence overall programme cost.

The parametric study was taken up to find the minimum thickness of web. It involved a number of manual iterations. The parameters chosen for design were 't_1' which is the thickness of web, 't_2' being the thickness of blade land and 't_3' the thickness of shaft hub as shown in the Figure 5.12. A few iterations in the beginning were tried with 't_1' = 7.5 mm, 8 mm and 8.5 mm thickness based on experience. These designs were out of thought as they were showing a high level of stress which is not acceptable as a solution. A thickness of 10 mm seemed to be the safe solution in terms of stress levels but still some optimization was required to bring the stress levels near its margin. Finally a minimum thickness of hub was iterated out to be 9.054 mm. The other thickness 't_2' and 't_3' were finalized to 3 and 4 mm respectively.

Upon finalising the minimum thickness the structural analysis was performed and it was observed that the stress distribution over the web portion of the blisk was non-uniform. This was again a matter of concern as the varied stress distribution may lead to weaker sections on a long run.

In order to overcome the weakening effect, a blisk of uniform strength was designed by shape morphing as shown in the Figure 5.13

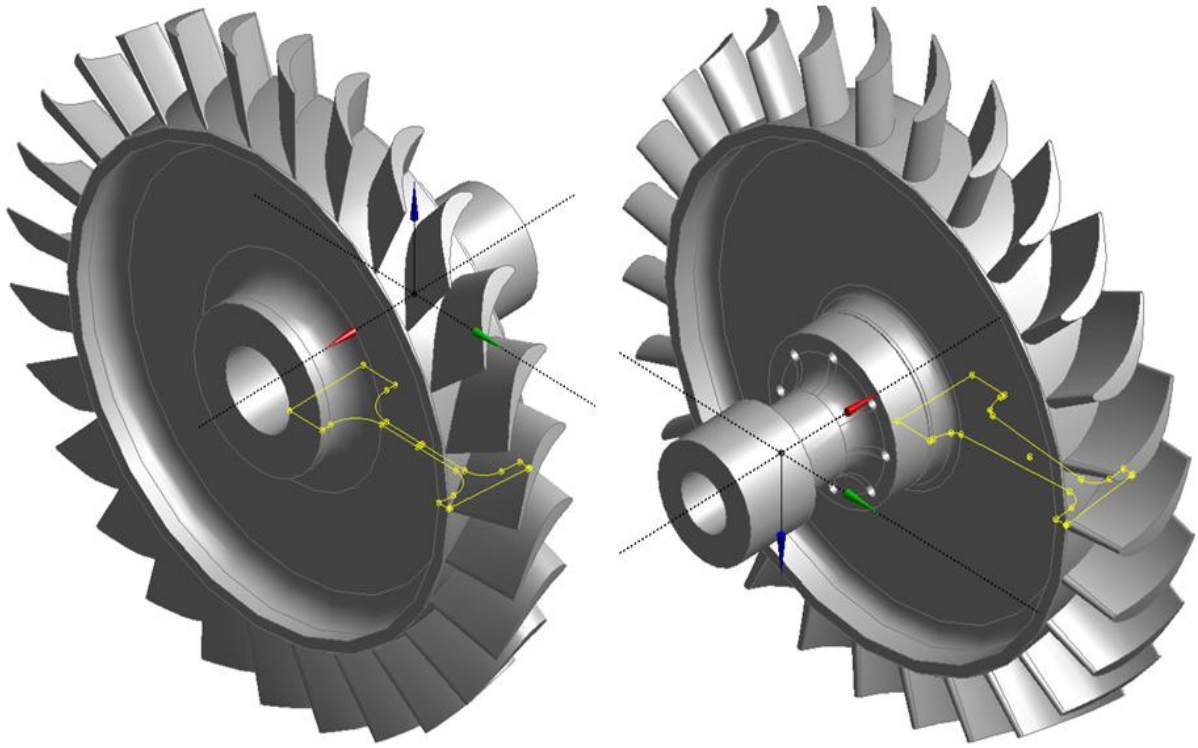

Figure 5.9 Blik of (a) Uniform Thickness and (b) Uniform Strength

6.5.2 Turbine Blisk Optimization

The main objective of optimization was to minimize the disc weight but still keeping stress levels within the yield limits of the material at the operating temperature of 1000 K. The problem variables for weight optimization included only two disc shape parameters: web thickness and hub radius at the shaft end. The optimisation plan involved an optimization technique called Design of experiments. As a starting design point, the optimizer was deliberately given a design band of variation for each input parameters that generated a diverse solution for the disc.

Among all the feasible solution satisfying all of the output constraints and objectives the one that yielded minimum weight for a marginal stress value was selected to be the optimal design as is shown in the Figure 5.14 The solution was obtained in approximately 6 hours on a 1GB ram system to converge at a solution.

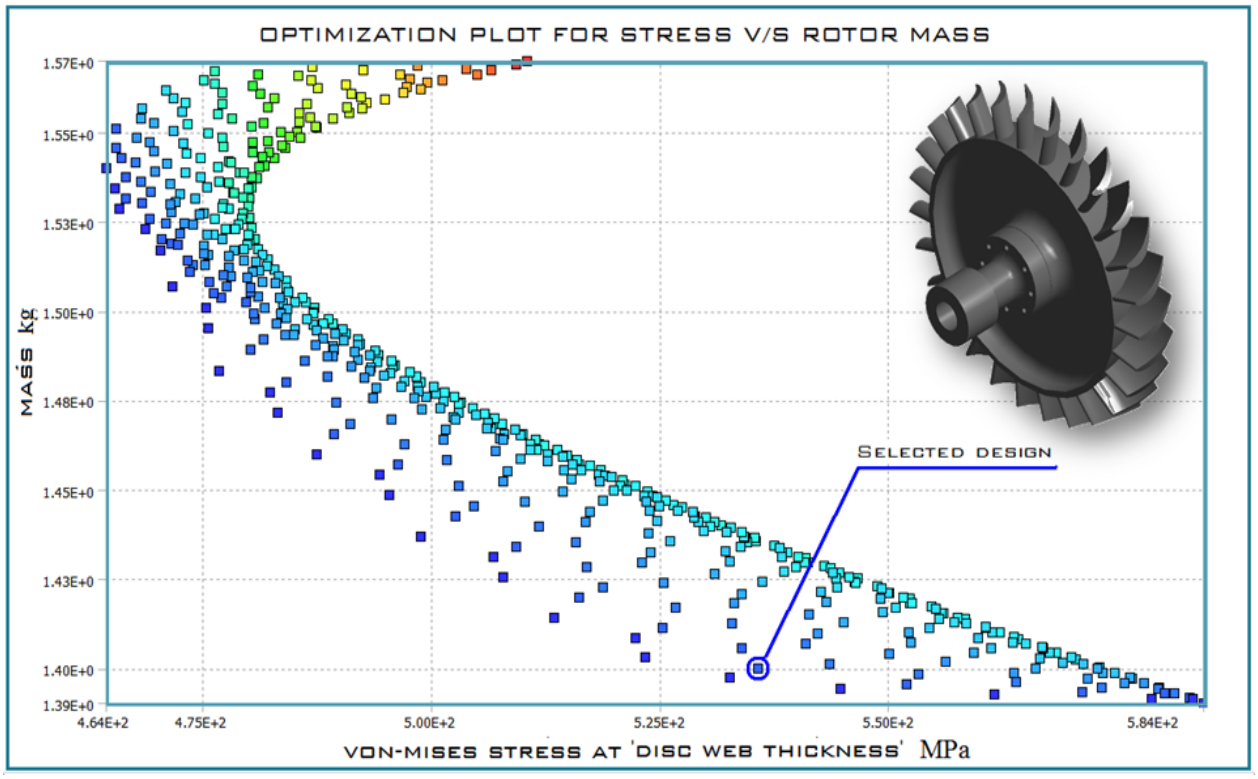

Figure 5.10 Weight Optimization of Shape Morphed Blisk

6 – Conclusions

Based on the design, analysis and optimization of the axial turbine stage presented in the previous sections, the following conclusions can be drawn:

6.1 Conclusion

- An axial flow Gas Generator Turbine stage is designed for an APU of fighter aircraft. The turbine develops a power of 319 kW. The turbine runs at 43000 rpm.
- A design space was created to obtain a design point 'P' that met the expected performance criteria in terms of stage reaction (45.5%) and efficiency (90.01%). The other design features at the design point involved an aerodynamic loading < 4.0, exit swirl angle of 20°, mean blade speed < 315 m/s and un-choked nozzles.
- A preliminary design code is developed based on free vortex theory and the preliminary design results form the basis of the blade creation process.
- The results obtained from CFD computations are in good agreement with design targets of thermodynamic cycle and preliminary design. A mass flow rate of 1.964 kg/s is obtained as against expected mass flow rate of 1.896 kg/s
- Studies on tip clearances were carried out and it is found that the minimum tip clearance of 1% resulted in best performance of the turbine.
- Studies with various stagger angles (30° to 45°) for NGV were carried out and it was found that the stagger angle of 40° gives the best performance without choking.
- MAR M 240 was selected as the material of the rotor blisk to meet the requirements of turbine operation at high temperature of 1200 K and un-cooled blades.
- Mechanical analysis of blisk was carried out both at the design speed and the burst speed of 115% and the stress levels were found well within the limits.
- Design optimization on the blisk was carried out for its weight and a disc of 1.4 kg was selected as the optimal design, keeping the stress levels within allowable limits.
- Shape morphing of the blisk was performed and the blisk of uniform strength was generated.

- An integrated approach of preliminary design, CFD analysis and mechanical analysis was followed and the results demonstrate the utility of the above design approach.

6.2 Recommendations for Future Work

- To carry out unsteady CFD analysis of turbine stage.

  The unsteady analysis of the turbine is required in order to assess its functionality under varied thermal pulses, change in operating conditions due to attitudes, etc.

- To carryout manufacturing and testing of the turbine design.

  The manufacturing and testing of prototype will be taken up in order to validate the design and to obtain the airworthiness certification.

- To estimate the life of the various subsystems of turbine stage.
- To select appropriate bearings for the Gas Generator turbine stage.

References

[1] "Gas Turbine Theory" by H.I.H. Saravanamuttoo, G.F.C. Rogers and H. Cohen,

Pearson Education, 2001, 5th ed., ISBN 0-13-015847-X.

[2] Panchenko, Y., Moustapha, H., Mah, S., Patel, K., Dowhan, M. J., Hall, D., (2002) "Preliminary Multi-Disciplinary Optimization in Turbomachinery Design", RTO-MP-089.

[3] "Aircraft Gas Turbine Technology" by Irwin E. Treager, Professor Emeritus

Purdue University, McGraw-Hill, Glencoe Division, 1979, ISBN 0070651582.

[4] *"The Jet Engine",* Rolls Royce plc, ISBN 0 902121 2 35

[5] Stepanoff, A.J., Theory, Design, and Application of Axial Flow Turbines. John Wiley & Sons, Inc, New York

[6] Calantuoni, S., Collella, A., Santoriello, G., Cirillo, L., lossa, C., (1993) "Aerothermal Design of 1600 K TET Core Engine Hot Section Components for High Technology Compact Propulsion Systems" AGARD-CP-537, ISBN 92-835-0738-X

[7] "Model Jet Engines" by Thomas Kamps ISBN 0 9510589 9 1 Traplet Publications

[8] Silet, J., (1993) "Specificite des groupes auxiliaires de puissance par rapport aux turbomoteurs d'helicoptere", presented at "Technology requirements for Small Gas Turbines", AGARD – CP – 537, ISBN 92-835-0738-X.

[9] Vinci, C., Campo, E., Trovati, A., (1993) "The Development of an Auxiliary Power Unit for a Fighter Aircraft", AGARD – CP – 537, ISBN 92-835-0738-X

[10] Trazzi P.E., (2004) "Design and Development of a 70 N Thrust Class Turbojet Engine", Engenharia Termica (Thermal Engineering), Paper No 5.

[11] Pierret, S., and Braembussche Van den, R.A., (1999) "Turbomachinery Blade Design

using a Navier-Stokes Solver and Artificial Neural Network", RTO-MP-8, AC/323(AVT)TP/9, ISBN 92-837-0005-8

[12] Vance, J.M., "Rotor dynamics of Turbomachinary" John Wiley & Sons, Inc, New York

[13] Materials Solutions 98, Gas Turbine Material Technology, Conference Proceeding from material solution 98, Pub. ASM International, (1998).

[14] Koul, A.K., (1993) "Hot Section Materials for Small Turbines", AGARD – CP – 537, ISBN 92-835-0738-X.

[15] Denton, J. D., (1994) "Axial turbine aerodynamic design", Lecture note for an advanced course on Turbomachinery Aerodynamic, University of Cambridge, UK

[16] M.EI.Masri, 1986 "Thermodynamics of Gas Turbine Cycle, Part 2" ASME J.Eng. Gas Turbine and Power, pp. 151-162.

[17] Schmidt Jameson, W., and Turkel, E., (1981) "Numerical Solution of Euler Solution by finite volume methods with Runge-kutta time stepping schemes", AIAA paper 81-1259

[18] http://www-materials.eng.cam.ac.uk/mpsite/, Dated 25 March 2009.

Appendix-A

General information on Materials [21]

- Figure A-1 shows the yield strength in tension for all materials.
- Maximum service temperature indicates the maximum temperature at which a material can be used and above this temperature, its strength rapidly decreases
- This chart is useful for identifying materials for components which operate at temperatures above room temperature.

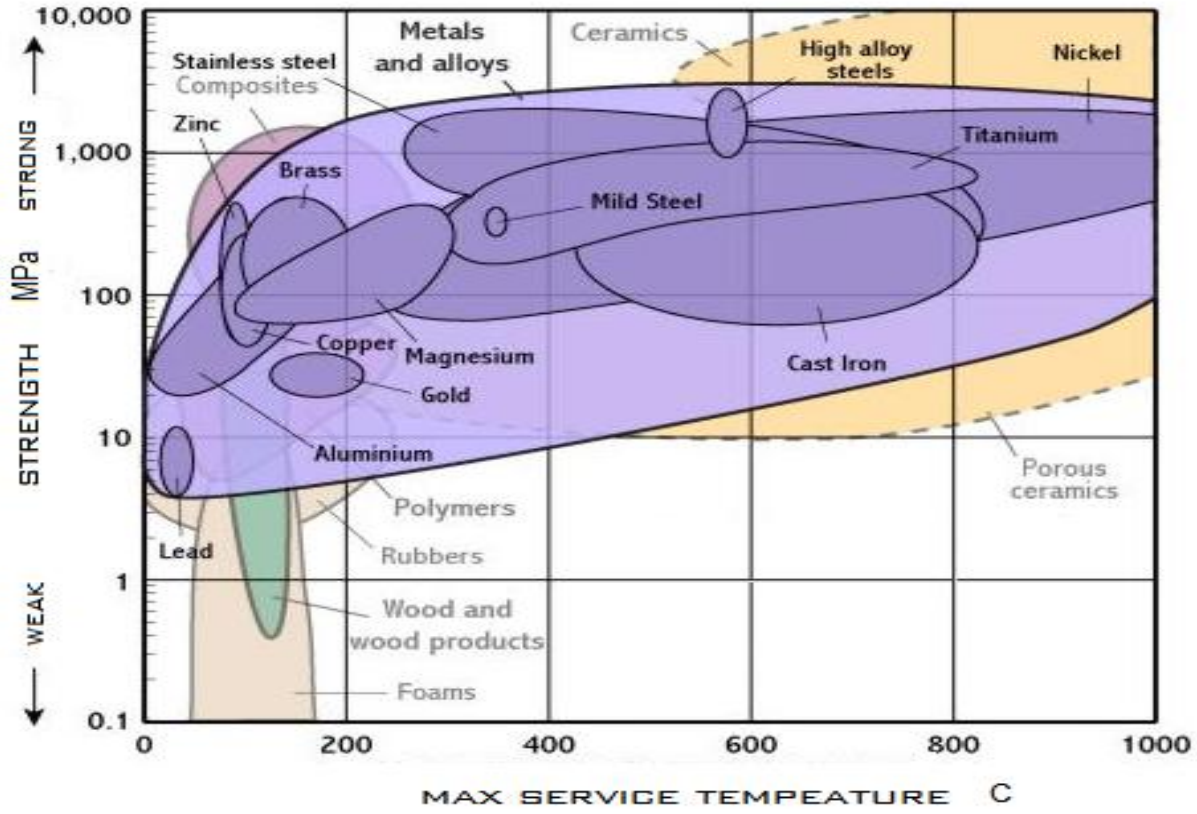

Figure A.1 Strength versus Max Service Temperature for Metals [21]

TABLE 1: PARAMETRIC STUDIES ON TURBINE CONFIGURAION

		U	314.79	m/s
		r	0.070	m
blade angle, α	20	blade loading	3.404	
		reaction	0.457	
Blade Speed, U	314.79	Limit of choke is 1.845	1.672	
		no of stator blades	11	
Aspect ratio, h/c	0.7	no of rotor blades	14	
		tip speed	398.7	
flow coefficient, φ	0.845			
		h0	0.021	m
		h1	0.028	m
		h2	0.037	m

Units: all velocities in m/s, dimensions in meter and Reaction in %

DESIGN SPECIFICATION TABLE

Mass Flow Rate	$\dot{m}$	1.896	kg/s
Isentropic Efficiency	η	0.88	-
Turbine Inlet Temperature	$T_{t1} = T_{t0}$	999.42	K
Temperature Drop across the stage	$\Delta T_{os} = (T_{01} - T_{03})$	147.89	K
Pressure ratio	P_{01} / P_{03}	2.0579	-
Inlet pressure	P_{01}	249013	Pa

DERIVED PARAMETERS TABLE

1	Rotational Speed		43078.97334	RPM
2	Rotor exit pressure	P_{t2}	121003.45	Pa

N

LIST OF ASSUMPTIONS

1	Mean Blade speed	U	314.7928994	m/s
2	Flow coefficient	ϕ	0.845	-
3	Angular velocity	ω	4511.219539	rad/s
4	Mean Radius of turbine	r_m	0.070	m
5	Pressure at rotor	$P_{t1}P_{t1}$	148913.937	Pa
7	Cutoff sp. speed for turbine design	N_s	0.76	-
8	flow velocities are constant	$C_{a1} = C_{a2}$	266	m/s
9	Inlet to nozzle=exit of rotor	$C_0 = C_2$	283.07	m/s

ADDITIONAL DATA AND INFORMATION

1	Specific heat at constant pressure	C_p	1140.4	J/kg-K
2	Specific heat ratio	γ	1.3362	-
3	Gas Constant	R	287	J/kg-k
4	Blade aspect ratio	$\lambda_{stator} = \lambda_{rotor}$	h/c	0.7

DESIGN CALCULATIONS

1 INVESTIGATION OF THE STAGE COUNT

$$\eta_t = \frac{1-\left[T_{t,ex}/T_{t,in}\right]}{1-\left[P_{t,ex}/P_{t,in}\right]^{(\gamma-1)/\gamma}}$$

$$T_{t,ex} = \left[1-\eta_t\left[1-\left[P_{t,ex}/P_{t,in}\right]^{(\gamma-1)/\gamma}\right]\right]\cdot\left[T_{t,in}\right]$$ 853.380 K

$T_{t,ex}$	Specified in statement of problem	999.420	K
$P_{t,ex} = P_{t,in}/\mathrm{Pr}.ratio$		121003.450	Pa
$\rho_{ex} \approx \rho_{t,ex} = \frac{P_{t,ex}}{RT_{t,ex}}$		0.422	kg/m^3
$\Delta h_{t,id} = C_p T_{t.in}$	Stage enthalpy drop	168653.756	J/kg
$N_s = \frac{\omega\sqrt{\dot{m}/\rho_{ex}}}{\Delta h_{t,id}^{3/4}}$		1.15	-

1.1 WORK SPLIT RATIO CALCULATIONS

$$x + y = 1$$
$$x/y = 440.676/315.60 = 1.396$$ 58.25:41.73
$$1.396y + y = 1$$
$$y = 0.4173, x = 0.5825 \Rightarrow Work\ Split\ Ratio = 58.25 : 41.73$$

1.2 Blade loading coefficient (Temp drop coefficient or Stage work coefficient)

$$\psi = \frac{2C_p \Delta T_{os}}{U^2}$$ 3.40 -

2.1.2 Flow kinematics - Stage 1- loop 2

The exit swirl angle is set to 20° 20.000 Deg

$$Tan\beta_2 = Tan\alpha_2 + \frac{1}{\phi} \quad \because \quad Tan\alpha_2 = Tan\beta_2 - \frac{1}{\phi}$$

$$\beta_2 = Tan^{-1}\left[Tan\alpha_2 + \left(\frac{1}{\phi}\right)\right]$$ 1.547 -

57.13 Deg

2.2.1 Reaction of the Turbine

$$R = \phi \tan\beta_2 - \frac{\psi}{4}$$ 0.46 Reaction

2.2.2 Blade loading coefficient (Also called Temperature drop coefficient or Stage work coefficient)

$$\beta_1 = Tan^{-1}\left(\frac{1}{2\phi}\left(\frac{1}{2}\psi - 2R\right)\right) \quad \because \quad Tan\beta_1 = \frac{1}{2\phi}\left(\frac{1}{2}\psi - 2R\right)$$ 25.020 Deg

$$\alpha_1 = Tan^{-1}\left(Tan\beta_1 + \frac{1}{\phi}\right)$$

$$\because \quad Tan\alpha_1 = Tan\beta_1 + \frac{1}{\phi}$$ 58.784 Deg

3	Verification of Non supersonic mach number: Velocities and angles:		
	$V_z = U\phi, \because \phi = V_z / U$	266.000	m/s
	$V_1 = \left[\frac{V_z}{Cos\alpha_1}\right]$	513.253	m/s
	$T_{01} - T_1 = \frac{V_1^2}{2C_p}$		
	$T_1 = T_{01} - \frac{V_1^2}{2C_p}$	115.498	K
	$T_1 - T_1^1 = \lambda \frac{V_1^2}{2C_p}$	883.922	K
	$T_1^1 = T_1 - \lambda \frac{V_1^2}{2C_p}$	5.775	K
		878.147	K

4	Verification of the stator and rotor choking status		
	$\frac{P_{00}}{P_1} = \left[\frac{T_{01}}{T_1^1}\right]^{\frac{\gamma}{\gamma-1}}$	$\Pr.ratio =$ 1.672	-
	$\frac{P_{00}}{P_c} = \left[\frac{\gamma+1}{2}\right]^{\frac{\gamma}{\gamma-1}}$	$P_1 =$ 148913.937	Pa
		$\Pr.ratio =$ 1.854	-

Comparing the PR obtained, 1.672 < 1.854 Nozzles are not choking now

$\rho_1 = \frac{P_1}{RT_1}$ 0.587 kg/m^3

$A_1 = \frac{m}{\rho_1 V_Z}$ 0.012 m^2

$A_{1N} = \frac{m}{\rho_1 V_1} = A_1 Cos\alpha_1$ 0.006 m^2

$V_{z0} = V_0 = V_2 = V_{z2} / Cos\alpha_2$ 283.071 m/s

$\frac{V_0^2}{2C_p}$ 35.132 K

$T_0 = T_{00} - \frac{V_0^2}{2C_p}$ 964.288 K

$\frac{P_0}{P_{00}} = \left[\frac{T_0}{T_{00}}\right]^{\frac{\gamma}{\gamma-1}}$ $P_0 =$ 216000.530 Pa

$\rho_0 = \frac{P_0}{RT_0}$ 0.780 kg/m^3

$A_0 = \frac{m}{\rho_0 V_{Z0}}$ 0.009 m^2

$T_{02} = T_{00} - \Delta T_{0s}$ 851.530 K

$T_2 = T_{02} - \frac{V_2^2}{2C_p}$ 816.398 K

$\frac{P_2}{P_{02}} = \left[\frac{T_2}{T_{02}}\right]^{\frac{\gamma}{\gamma-1}}$

$P_2 =$ 102346.770 Pa

$\rho_2 = \frac{P_2}{RT_2}$ 0.437 kg/m^3

$A_2 = \frac{m}{\rho_2 V_Z}$ 0.016 m^2

5 Calculation of Annulus height

$U_m = 2\pi N r_m$

$r_m = \frac{U_m}{2\pi N}$

$h = \frac{AN}{U_m}$ $\quad A = 2\pi r_m h = \frac{U_m h}{N}$ 0.070 m

$h_0 = \frac{A_0 N}{U_m}$ 0.021 m

$h_1 = \frac{A_1 N}{U_m}$ 0.028 m

$h_2 = \frac{A_2 N}{U_m}$ 0.037 m

$\left(\frac{r_t}{r_r}\right)_{mean,0} = \frac{r_m + (h_0/2)}{r_m - (h_0/2)}$ mean design 1.351 -

$\left(\frac{r_t}{r_r}\right)_{mean,1} = \frac{r_m + (h_1/2)}{r_m - (h_1/2)}$ 1.495 -

$\left(\frac{r_t}{r_r}\right)_{mean,2} = \frac{r_m + (h_2/2)}{r_m - (h_2/2)}$

	1.727	-
$r_{0,tip} = r_m + h_0 / 2$	0.0802	m
$r_{1,tip} = r_m + h_1 / 2$	0.0836	m
$r_{2,tip} = r_m + h_2 / 2$	0.0884	m
$r_{0,hub} = r_m - h_o / 2$	0.0594	m
$r_{1,hub} = r_m - h_1 / 2$	0.0559	m
$r_{2,hub} = r_m - h_2 / 2$	0.0512	m

$\left(\frac{r_m}{r_h}\right)_{hub,0} = \frac{r_m}{r_m - (h_0/2)}$	1.175	-
$\left(\frac{r_m}{r_t}\right)_{tip,0} = \frac{r_m}{r_m + (h_0/2)}$	0.870	-
$\left(\frac{r_m}{r_h}\right)_{hub,1} = \frac{r_m}{r_m - (h_1/2)}$	1.248	-
$\left(\frac{r_m}{r_t}\right)_{tip,1} = \frac{r_m}{r_m + (h_1/2)}$	0.834	-
$\left(\frac{r_m}{r_h}\right)_{hub,2} = \frac{r_m}{r_m - (h_2/2)}$	1.364	-
$\left(\frac{r_m}{r_t}\right)_{tip,2} = \frac{r_m}{r_m + (h_2/2)}$	0.79	-

7 Summary of angles

1	Flow angle	α_{0m}	20	Deg
2	Flow angle	α_{1m}	58.784	Deg
3	Flow angle	α_{2m}	20.000	Deg
4	Flow angle	β_{0m}	0	Deg
5	Flow angle	β_{1m}	25.020	Deg
6	Flow angle	β_{2m}	57.128	Deg

8 Free Vortex Design

$$\alpha_{1,hub} = Tan^{-1}\left(\left[\frac{r_m}{r}\right]_1 Tan\alpha_{1m}\right)$$ 64.092 Deg

$$\alpha_{1,tip} = Tan^{-1}\left(\left[\frac{r_m}{r}\right]_1 Tan\alpha_{m1}\right)$$

$$\alpha_{2,hub} = Tan^{-1}\left(\left[\frac{r_m}{r}\right]_2 Tan\alpha_{2m}\right)$$

$$Tan^{-1}\left(\left[\frac{r_m}{r}\right]_2 Tan\right)$$

54.011 Deg

26.397 Deg

$$\beta_{1,hub} = Tan^{-1}\left(\left[\frac{r_m}{r_h}\right]_1 Tan\alpha_{1m} - \left[\frac{r_h}{r_m}\right]_1 \frac{U_m}{V_{z1}}\right)$$ 16.032 Deg

$$\beta_{1,tip} = Tan^{-1}\left(\left[\frac{r_m}{r_t}\right]_1 Tan\alpha_{1m} - \left[\frac{r_t}{r_m}\right]_1 \frac{U_m}{V_{z1}}\right)$$ 47.988 Deg

$$\beta_{2,hub} = Tan^{-1}\left(\left[\frac{r_m}{r_h}\right]_2 Tan\alpha_{2m} + \left[\frac{r_h}{r_m}\right]_2 \frac{U_m}{V_{z2}}\right)$$ -2.368 Deg

$$\beta_{2,tip} = Tan^{-1}\left(\left[\frac{r_m}{r_t}\right]_2 Tan\alpha_{2m} + \left[\frac{r_t}{r_m}\right]_2 \frac{U_m}{V_{z2}}\right)$$ 52.682 Deg

60.760 Deg

Summary of all the angles

	α_1	β_1	α_2	β_2
Tip	54.011	-2.368	16.032	60.760
Mean	58.784	25.020	20.000	57.128
Hub	64.092	47.988	26.397	52.682

1 Mean radius, axial chords and stator/rotor gaps, Optimal no of blades

From Graph, the ratio of (s/c) for stator	0.820	
From Graph, the ratio of (s/c) for rotor	0.810	
$h_N = 0.5(h_0 + h_1)$	0.024	m
$h_R = 0.5(h_2 + h_1)$	0.032	m
$c_N = h_N$	0.035	m
$c_R = h_R$	0.046	m

zweifel's loading criterion at the mean radius=0.8

$$0.8 = (\psi_z)_{opt} = 2\left[\frac{S_m}{C_{zm}}\right] Cos^2\beta_2 [Tan\beta_1 - Tan\beta_2]$$

$$S_m = \frac{C_{zm}(\psi_z)_{opt}}{2Cos^2\beta_2[Tan\beta_1 - Tan\beta_2]}$$ ROTOR — 0.0313 m

$$N_b = \frac{2\pi r_m}{S_m}$$ — 14.027 Nos.

$$S_m = \frac{C_{zm}(\psi_z)_{opt}}{2Cos^2\beta_2[Tan\beta_1 - Tan\beta_2]}$$ STATOR — 0.0401 m

$$N_b = \frac{2\pi r_m}{S_m}$$ — 10.925 Nos.

chord for nozzles — 0.035 m

$$s_N = c_N(x)$$

chord for blades	0.046	m
	0.028	m
$s_R = c_R(y)$	0.038	
$n_b = 2\pi r_m / s$	15.43	Nos
$n_b = 2\pi r_m / s$	11.67	Nos

Rotor Blade stress

Density of Ni-Cr-C0	8000.000	kg/m^3
$A = 0.5(A_1 + A_2)$	0.014	m^2
$(\sigma_{ct})_{\max} = \frac{4}{3}\pi N^2 \rho A$	245.8	MN/m^2
$\beta_{1r} + \beta_{2r}$	100.7	Deg
$m(V_{w1m} + V_{w2m}) = mV_z(Tan\alpha_1 + Tan\alpha_2)$	1015.8	N
$(\sigma_{gb})_{\max} = \frac{m(V_{w1m} + V_{w2m})}{n}\frac{h}{2}\frac{1}{zc^3}$		

	3.349	MN/m^2
Torque	70.88	NM
Power	319.76	KW

SUMMARY OF ALL ANGLES

r_t / r_h	α_0	β_0	α_1	β_1	α_2	β_2
Tip	17.62	17.62	54.010694	-2.36832	16.031545	60.760195
Mean	20	20	58.784196	25.020197	20.000	57.127661
Hub	23.215	23.215	64.092309	47.987678	26.39676	52.681993

SUMMARY OF PROPERTIES AND DIMENSIONS

Plane	0	1	2
P	216000.5	148913.9	102346.8
T	964.3	883.9	816.4
Density	0.780	0.587	0.437
A	0.009	0.012	0.016
mean rad	0.070	0.070	0.070
	1.351	1.495	1.727
h	0.021	0.028	0.037

Blade row	Nozzle	rotor
s/c	1.1578	0.6741
mean h	0.0243	0.0325
h/c	0.7000	0.7000
c	0.0347	0.0464
s	0.0401	0.0313
n	10.9250	14.0269

Vel	Mag	Unit	Vel	Mag	Unit
V_0	283.07	m/s	$U_{MEAN,1}$	314.79	m/s
V_1	513.25	m/s	$U_{MEAN,2}$	314.79	m/s
V_2	283.07	m/s	$U_{TIP,1}$	377.26	m/s
V_{z0}	266.00	m/s	$U_{TIP,2}$	398.74	m/s
V_{z1}	266.00	m/s	$U_{HUB,1}$	252.32	m/s
V_{z2}	266.00	m/s	$U_{HUB,2}$	267.81	m/s